https://doi.org/10.5194/acp-2022-490
Preprint. Discussion started: 4 October 2022

Atmospheric Chemistry and Physics Discussions

Understanding day-night differences in dust activities over the dust belt of North Africa, the Middle East, and Asia

Jacob Zora-Oni Tindan, Qinjian Jin, Bing Pu

Department of Geography and Atmospheric Science, University of Kansas, Lawrence, KS, USA

Correspondence to: Jacob Zora-Oni Tindan (jtindan@ku.edu), Bing Pu (bpu@ku.edu)

Abstract. Utilizing the well-calibrated, high spectral resolution, and equal-quality-performance for day and night observations (9:30 a.m. and 9:30 p.m. equator passing time) of the Infrared Atmospheric Sounder Interferometer (IASI) products, this study investigates the day-night differences in dust activities over the dust belt of North Africa, the Middle East, and Asia. Both daytime and nighttime dust optical depth (DOD) at 10 μm shows high consistency with solar and lunar observations from AErosol RObotic NETwork (AERONET) sites across the dust belt, with correlation coefficients of 0.8–0.9 for most sites. IASI reveals significant (95% confidence level) day-night differences in dust activities over the major dust sources within the dust belt. Annual mean daytime DOD at 9:30 a.m. is significantly higher than that of nighttime at 9:30 p.m. in the central to northern Sahara Desert, the central to eastern Arabian Peninsula and dust source regions in South and East Asia including the Taklamakan Desert, but lower over the southern Sahel to the Guinea Coast, and the central to southern Indian subcontinent. The magnitude of the day-night difference in DOD is larger and more significant in boreal winter and spring than other seasons. An analysis of 10 m wind fields and dust uplift potential using the European Centre for Medium-Range Weather Forecasts (ECMWF) Reanalysis v5 (ERA5) suggests that the positive day-night differences in DOD over the central Sahara, the Middle East, and Asia are associated with enhanced dust emissions driven by stronger wind speed. Dust layer heights demonstrate negative day-night differences (i.e., lower daytime versus higher nighttime values) over dust source regions in the central Sahara, central Arabian Peninsula, and Asia, and positive height differences in the southern Sahel to the Guinea Coast, southern parts of the Arabian Peninsula, and large parts of the Indian subcontinent. The higher dust layer height over the Guinea Coast and the Indian subcontinent during daytime is associated with a deeper planetary boundary layer height and greater convective instability around 9:30 a.m. than that during 9:30 p.m., which promotes vertical transport and mixing of dust. The corresponding lower daytime DOD over these downwind regions indicates a possible dilution of dust aerosols when they are transported to higher altitude by convections and are more susceptible to horizontal transport.

Ground observations from the Laboratoire Interuniversitaire des Systèmes Atmosphériques (LISA) and AERONET show surface PM_{10} concentration and dust aerosols exhibit a spatially varying diurnal cycle across the dust belt with peak coarse-mode aerosol optical depth (CAOD; around 7–9 a.m.) and PM_{10} concentrations (around 9–11 a.m.) in the morning hours and late afternoon to midnight in the Sahel, peak CAOD from morning to early afternoon (around 9 a.m.–1 p.m.) and around midnight in the Middle East and Asia, generally consistent with day-night differences in dust activities revealed by IASI.

An examination of DOD from Modern-Era Retrospective Analysis for Research and Applications, version 2 (MERRA-2) and ECMWF Atmospheric Composition Reanalysis 4 (EAC4) products reveals that reanalysis products largely

https://doi.org/10.5194/acp-2022-490
Preprint. Discussion started: 4 October 2022


Atmospheric Chemistry and Physics Discussions

capture the temporal and spatial variability of DOD on the seasonal scale but failed to capture the day-night differences in DOD in large parts of the dust belt except in a few dust source hotspots over North Africa, such as the northeastern Bodélé Depression and the northeastern North Africa. Overall, this study provides a detailed and comprehensive analysis of the day-night differences in dust activities over the dust belt, which could improve our current understanding of physical mechanisms of dust cycle at the diurnal timescale in various dust source and downwind regions.

1 Introduction

Mineral dust is one of the primary aerosols in the atmosphere and forms an integral part of the climate system. It is produced mainly by wind erosion in deserts, dry lake beds, arid and semi-arid regions (Penner et al., 2001), and their uplift in source regions mostly occur when the surface wind speed, which is also affected by land surface characteristics and vegetative cover, exceeds a suitable threshold (Fernandez-Partagas et al., 1986; Marsham et al., 2008; Bergametti et al., 2017; Pu et al., 2020). The global emission of dust aerosols is estimated to range between 1000 and 5000 Tg yr^{-1} with high spatiotemporal variability due to its relatively short atmospheric lifetime (Duce, 1995; Ginoux et al., 2001; Huneeus et al., 2011; Checa-Garcia et al., 2021). North Africa alone accounts for about 50% of the global dust emissions (Schütz, 1980; D'Almeida, 1986; Tegen and Fung, 1994; Swap et al., 1996; Ginoux et al., 2012; Kok et al., 2021), followed by the Middle East and Asia contributing about 40% of global dust emissions (Prospero et al., 2002; Goudie and Middleton, 2006; Tanaka and Chiba, 2006; Huneeus et al., 2011; Kok et al., 2021).

Dust aerosol impacts atmospheric radiative balance directly by dust–radiation interactions and indirectly by dust–cloud interactions, the effect of which serves as one of the largest sources of uncertainties in modelling aerosol effects and global climate change (Forster et al., 2007; Haywood et al., 2005; Mahowald et al., 2010). The radiative effect of dust refers to its scattering and absorption of incoming shortwave and outgoing longwave radiation, consequently affecting regional climate, e.g., African and Indian monsoon systems (Miller and Tegen, 1998; Li et al., 2004; Mahowald et al., 2010; Jin et al., 2014, 2015, 2016, 2021) and tropical cyclones in the North Atlantic (Karyampudi and Carlson, 1988; Dunion and Velden, 2004; Wong and Dessler, 2005; Strong et al., 2018). Dust aerosols can also modify the macro– and micro–physical properties of clouds by serving as cloud condensation and ice nuclei, namely aerosol–cloud interactions that can further interact with the hydrological cycle (Levin et al., 1996; Rosenfield et al., 1997; Nakajima et al., 2001; DeMott et al., 2003; Bangert et al., 2012). Dust aerosols affect continental and maritime ecosystems by providing nutrients such as phosphorus, iron, and nitrogen (Duce and Tindale, 1991; Mills et al., 2004; Okin et al., 2004). For instance, African dust has been found to influence ecosystems in the Amazon Basin (Swap et al., 1992; Bristow et al., 2010; Yu et al., 2015) and the Atlantic Ocean (Jickells et al., 2005; Mahowald et al., 2010).

Quantifying the climatic impacts of dust requires accurate and detailed information on their spatial and temporal distributions. In addition to seasonal, interannual, and decadal timescales of variability, the diurnal variation in dust is also an important aspect that has been explored by many works. Past studies reveal significant daytime and nighttime variabilities in

https://doi.org/10.5194/acp-2022-490
Preprint. Discussion started: 4 October 2022


Atmospheric Chemistry and Physics Discussions

dust loading over the dust belt (Wang et al., 2004; Schepanski et al. 2009; Fiedler et al., 2013; Heinold et al., 2013; Kocha et al., 2013; Osipov et al., 2015; Yu et al., 2016; Chédin et al., 2020; Yu et al., 2021). For example, in North Africa, pronounced dust emissions during the morning hours of the day are found to be associated with the breaking down of the nocturnal low–level jets (Engelstaedter et al., 2006; Todd et al., 2008; Tulet et al., 2010; Knippertz and Todd, 2012) and in the late afternoon period as a result of mesoscale convective systems leading to dust emissions at the leading edge of density currents (Flamant et al., 2007; Marsham et al., 2008; Todd et al., 2008; Knippertz and Todd, 2012). Satellite observations and regional model simulations in West Africa showed a well-marked diurnal variability of dust associated with a rising planetary boundary layer maximizing at about 15 UTC (Coordinated Universal Time; about 4 p.m. local solar time (LST)) (Chaboureau et al., 2007). Using the fifteen-minute Meteosat Second Generation (MSG) Spinning Enhanced Visible and Infrared Imager (SEVIRI) satellite product, Schepanski et al. (2009) found about 65% of the dust source activation in the Sahara Desert occurring between 0600 and 0900 UTC.

In the Middle East, summertime dust emissions are primarily caused by the strong, persistent Shamal winds which maximize around local noon over the Iraqi Desert (Yu et al., 2016). Around the Gobi and Taklamakan deserts in Asia, dust emissions in spring to early summer show a diurnal change of more than ±10% Aerosol Optical Depth (AOD) and ±30% of Angström exponent, with larger AOD and smaller Angström exponent values in late afternoon (Wang et al., 2004). Smirnov et al. (2002) showed a prevailing pattern of AOD increase by 10%–40% during the daytime over dust sources in North Africa and Asia with less diurnal variability over regions where dust aerosol is a major contributor to the total AOD. By analysing aerosol extinction and typing profiles from Cloud-Aerosol Transport System (CATS) lidar on a global scale, Yu et al. (2021) identified a significant daytime and nighttime variations in dust and dust mixture loading over the major dust sources in North Africa, and western and southern North America.

However, observations of the full diurnal cycle of dust with a global coverage is still lacking. Ground-based instruments such as AERONET (Holben et al., 1998; O'Neill et al., 2003) and LISA stations over the Sahel (Marticorena et al., 2010) have high temporal resolution (~15 minutes for AERONET and an hour for LISA), but with low spatial coverage. On the other hand, while satellite products have much higher spatial resolutions and coverage, polar-orbiting instruments have low temporal coverage, i.e., two times daily. Moreover, most of these instruments (both satellite and ground-based) sample aerosols based on the measurement of radiance in visible bands, making it difficult to observe dust events in the nighttime and thereby missing out some important characteristics of dust. For instance, widely used products, such as, the Moderate Resolution Imaging Spectroradiometer (MODIS) onboard both the Terra and Aqua satellites and Multi-angle Imaging SpectroRadiometer (MISR; Diner et al., 1998) onboard the Terra satellite retrieve AOD once per day only in visible wavelengths. Observations from lidar instruments such as Cloud-Aerosol Lidar with Orthogonal Polarization (CALIOP; Winker et al., 2009) provide vertically resolved aerosol extinction and clouds for snapshots during both daytime (1:30 p.m.) and nighttime (1:30 a.m.). However, CALIOP has two significant drawbacks when it is used to study day-night differences of DOD: (1) A lower signal-to-noise ratio during the daytime than nighttime, making it less sensitive to daytime observations (Liu et al., 2009) and less reliable to directly compare its daytime and nighttime products and (2) A narrow horizontal swath of 5

https://doi.org/10.5194/acp-2022-490
Preprint. Discussion started: 4 October 2022


Atmospheric Chemistry and Physics Discussions

km, which means there is only one daily observation at a specific location thus no day-night differences of DOD can be retrieved at daily timescale. SEVIRI instrument (Schmetz et al., 2002; Schepanski et al., 2007, 2009) aboard the Meteosat Second Generation satellite, which is a geostationary satellite located at 3.5°W above the equator, provides dust observations from infrared (IR) channels every 15 minutes. However, this product mainly covers Africa and the Arabian Peninsula. The above challenges are partly addressed by the Infrared Atmospheric Sounder Interferometer (IASI).

IASI sensor onboard the European Meteorological Operational satellite (MetOP) provides retrievals of dust optical depth (DOD) and dust layer height at IR bands twice per day (9:30 a.m. and 9:30 p.m.) at global scale (Blumstein et al., 2004; Capelle et al., 2014, 2018), facilitating the study of day-night differences in dust activities. It has a fine spectral and spatial resolutions of 0.5 cm^{-1} and 12 km at nadir, respectively, as well as showing high quality in capturing the spatiotemporal variability of dust (Hewison et al., 2013) in comparison to ground measurements from AERONET (Capelle et al., 2014, 2018). The observation time of IASI generally coincides with the two dominant dust generation mechanisms in north Africa, the breaking down of the nocturnal low–level jets in the early morning hours and mesoscale convective systems in the evening period (Engelstaedter et al., 2006; Washington et al., 2006; Knippertz and Todd, 2012; Chédin et al., 2020). One important advantage of IASI is its equal quality performance for daytime and nighttime observations (Hewison et al., 2013; Chédin et al. 2020), making it suitable to compare daytime and nighttime variability of dust. The data have been used to study characteristics of dust in the Sahara Desert (Chédin et al., 2018; 2020).

In this work, we will leverage on the strength of IASI together with in situ observations from AERONET and LISA sites (Berkoff et al., 2011; Holben et al., 1998; Marticorena et al., 2010) to understand daytime and nighttime variability of dust activities and their day-night differences over the dust belt of North Africa, the Middle East, and East Asia (Fig. 1). Aerosol reanalysis products, such as MERRA-2 (Gelaro et al., 2017; Randles et al., 2017) and ECMWF Atmospheric Composition Reanalysis 4 (EAC4; Inness et al., 2019), which are widely used in model validation and case studies (Grandey et al., 2013; Carmona et al., 2020; Isaza et al., 2021) as they assimilate total AOD from satellite products while providing high spatial and temporal coverage of dust distribution, are employed for comparative purpose with IASI results. We will examine whether these aerosol reanalysis products capture the day-night activities of dust shown in satellite products. Lastly, we will examine the meteorological conditions that contribute to the observed day-night differences in dust activities. Section 2 describes the study domain and introduces the datasets and data analysis techniques. Results are presented in section 3, and uncertainties are discussed in section 4. Major findings are summarized in section 5.

https://doi.org/10.5194/acp-2022-490
Preprint. Discussion started: 4 October 2022

Atmospheric Chemistry and Physics Discussions

2 Data and methodology

2.1 Study Domain

In this paper, we focus on the dust belt extending from North Africa through the Middle East and Central Asia to the deserts in western East Asia (Fig. 1). The Saharan dust belt (0–35°N, 16°W–25°E) is the world's largest source of aeolian desert dust aerosols, with an annual emissions of 400–700 × 10^6 tons of dust aerosols (D'Almeida, 1986; Schütz, 1980; Swap et al., 1996). There are two major dust sources within the Sahara — the Bodélé Depression and an area covering eastern Mauritania, western Mali and southern Algeria (Middleton and Goudie, 2001).

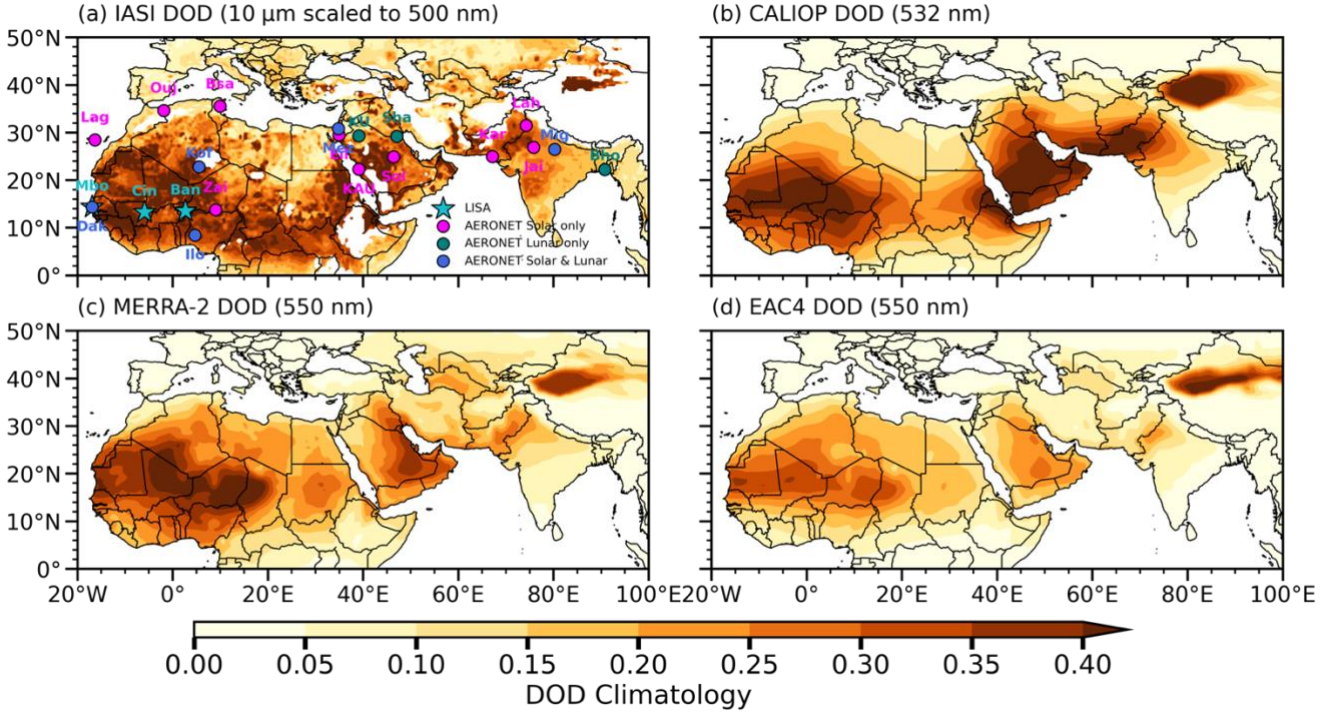

Figure 1: Climatology (2008–2020) of DOD from (a) IASI, (b) CALIOP, (c) MERRA-2 and (d) EAC4. Magenta, teal, and royal blue-colored dots represent AERONET sites with solar, lunar data, and both solar and lunar records, respectively. Cyan stars represent LISA sites. Note that IASI DOD in (a) represents the climatology of average daytime (9:30 a.m.) and nighttime (9: 30 p.m.) DOD is scaled from 10 µm infrared (IR) to 500 nm visible wavelength (VIS) using an IR/VIS ratio of 0.63 obtained by averaging all the IR/VIS ratios among AERONET sites in the domain (Table 2). Note that CALIOP data are up to July 2020.

The Middle East dust belt (13°N–38°N, 25°E–60°E) is the world's second largest dust source (Prospero et al., 2002; Goudie and Middleton, 2006; Huneeus et al., 2011; Kok et al., 2021). The Middle East and South Asian dust sources covers Sudan, the Arabian Peninsula, parts of Iran and Afghanistan, and Pakistan (Rezazadeh et al., 2013). The East Asian dust belt (7°N–46°N, 60°E–100°E) mainly includes the Taklamakan and the Gobi Deserts (Prospero et al., 2002) and is estimated to

https://doi.org/10.5194/acp-2022-490
Preprint. Discussion started: 4 October 2022


Atmospheric Chemistry and Physics Discussions

account for about 3%–11% of global dust emissions (Tanaka and Chiba, 2006). We did not include the Gobi Desert in our domain due to large area of missing data in IASI.

2.2 Datasets

This study mainly uses the 10 μm DOD retrieved from IASI as the primary dataset to understand the day-night differences in dust activities, e.g., DOD and dust plume layer height, in the dust belt, along with ground observations. Results from IASI are compared with aerosol products from reanalyses. Meteorological variables from reanalysis and stations are used to examine their influences on the day-night differences in dust activities. All the datasets used in this study are summarized in Table 1.

Table 1. Summary of datasets and variables used in this study

Variable	Dataset	Version	Period used	Spatial Resolution	Temporal Resolution	Link to data
DOD, dust layer height	IASI	2.20	2008-2020	12km	daily	https://iasi.aeris-data.fr/DUST-AOD_IASI_A_data/
DOD, dust layer height	CALIOP	4.20	2008-2020	5 km (5°×2°)	monthly	https://asdc.larc.nasa.gov/project/CALIPSO
CAOD	AERONET	2.0, 1.50	2008-2020	station	15 mins	https://aeronet.gsfc.nasa.gov/
PM_{10}	LISA	-	2008-2020	station	hourly	http://www.lisa.u-pec.fr/SDT/index.php?p=3
DOD	MERRA-2	-	2008-2020	0.625°×0.5°	hourly	https://disc.gsfc.nasa.gov/
DOD	EAC4	V4	2008-2020	80km	3-hourly	https://ads.atmosphere.copernicus.eu
Rainfall, PBLH, CAPE, circulations	ERA5	-	2008-2020	0.25°×0.25°	hourly	https://cds.climate.copernicus.eu/#!/home
Precipitation	IMERG	V06B	2008-2020	0.1°×0.1°	30 mins	https://gpm.nasa.gov/data/directory

2.2.1 IASI

IASI is a high spectral resolution thermal infrared Fourier transform spectrometer onboard MetOP-A, MetOP-B and MetOP-C satellites (Capelle et al., 2014, 2018; Chédin et al., 2020; Siméoni et al., 1997). It measures radiance over 8641 spectral channels extending from 645 to 2760 cm^{-1} with a spectral resolution of 0.5 cm^{-1}. It has a ground resolution of 12 km at nadir. Onboard MetOP-A at an altitude of about 800 km, IASI observes Earth at an angle of ~48.5° perpendicular to both sides of the satellite track. This corresponds to a swath width of ~2000 km leading to a global coverage in 12 hours. The satellite has a local equatorial crossing times of approximately 9:30 a.m. and 9:30 p.m. and is available from July 2007 to October 2021.

Due to its wide spectrum in longwave range and fine spectral resolution, IASI is widely used to retrieve atmospheric compositions during both day and night times. IASI dusty and cloudy pixels are distinguished using cloud mask based on nine screening tests consisting of infrared observations from both IASI and the Advanced Microwave Sounding Unit (AMSU) at same time and locations over the globe (Capelle et al., 2018). IASI DOD and dust layer height retrieved by the team from Laboratoire de Mètèorologie Dynamique (LMD; Capelle et al., 2018; Peyridieu et al., 2013) are used in this study due to its good consistency with in situ observations (Capelle et al., 2014, 2018; Peyridieu et al., 2013; Zheng et al., 2022). The retrieval

https://doi.org/10.5194/acp-2022-490
Preprint. Discussion started: 4 October 2022


Atmospheric Chemistry and Physics Discussions

of DOD and dust layer height from IASI cloud-free observations is based on an iterative two-step approach using different look-up tables (Capelle et al., 2018; Peyridieu et al., 2013). The first step determines the atmospheric state using 18 IASI channels, and the second step is retrieval of 10 μm DOD, dust layer mean altitude, and surface temperature simultaneously using the algorithm similar to that was originally applied to Atmospheric Infrared Sounder (AIRS; Peyridieu et al., 2010). Here, level 2 (version 2.2.0) daily 10 μm DOD and dust layer height at 9:30 a.m. and 9:30 p.m. (referred to daytime and nighttime, respectively) are used and regridded into a 0.5° by 0.5° grid from January 2008 to December 2020. Dust layer height is defined as the height at which half of the DOD is found above and the other half below (Capelle et al., 2018; Chédin et al., 2020).

2.2.2 CALIOP

CALIOP is a spaceborne two-wavelength polarization lidar onboard Cloud-Aerosol Lidar and Infrared Pathfinder Satellite Observation (CALIPSO) satellite. It provides high resolution vertical profiles of global clouds and aerosols measurements since June 2006 (Winker et al., 2009). CALIOP is a near-nadir viewing instrument which has a very narrow swath width i.e., a beam diameter of 70 m at the Earth's surface corresponding to a 16-day repetition cycle thus making its instantaneous field of view approximately 300 m and 70 m. Level 3 cloud-free monthly DOD at 532 nm and dust layer height on a 5° × 2° grid from 2008 to 2020 are used to compare with IASI. Note that because of the high altitude and modest power-aperture of CALIOP, its daytime product has an extremely low signal-to-noise ratio (Winker et al., 2017), making a direct comparison between daytime and nighttime products less reliable. Moreover, due to its narrow swath width, no day-night difference can be calculated at daily timescale. To compare with IASI dust layer height, we analyzed dust altitude from CALIOP by calculating the mean of the highest and lowest dust aerosol layer detected.

2.2.3 AERONET

AERONET is a ground-based sun photometer aerosol observation network established by the National Aeronautics and Space Administration (NASA) and PHOtométrie pour le Traitement Opérationnel de Normalisation Satellitaire (PHOTONS) which measures atmospheric aerosol properties globally (Holben et al., 1998). The sun photometers perform measurements of solar irradiance in eight spectral bands (340, 380, 440, 500, 670, 870, 940 and 1020 nm) in about every 15 minutes from 5 a.m. or 6 a.m. to 5 p.m. or 6 p.m. local solar time (LST; depending on the site). The lunar photometers perform nocturnal measurements from 5 p.m. or 6 p.m. to 5 a.m. or 6 a.m. LST with an approximate field of view of 1.29° at eight nominal wavelengths of 440, 500, 675, 870, 937, 938, 1020, and 1640 nm. The estimated uncertainty of AOD using direct solar radiation measurement is > ±0.01 for wavelength of > 0.44 μm and < ±0.021 for shorter wavelengths (Eck et al., 1999).

We use version 3 level 2 (cloud screened and quality assured) Spectral Deconvolution Algorithm (SDA; O'Neill et al., 2003) retrieval of the coarse mode AOD (CAOD; Eck et al., 2010) around 500 nm to approximate DOD and compare with IASI DOD. It is important to note that the SDA algorithm of AERONET CAOD is sensitive to the presence of high clouds such as cirrus and may lead to overestimation of AERONET CAOD (Smirnov et al., 2018). Over coastal regions, CAOD may

https://doi.org/10.5194/acp-2022-490
Preprint. Discussion started: 4 October 2022


Atmospheric Chemistry and Physics Discussions

contain information from sea salt as well. Level 2.0 data are not available at lunar sites, so level 1.5 data (cloud screened but not quality assured) are used.

Missing values in both solar and lunar records were removed before the analysis. Validation of IASI daytime and nighttime DOD against AERONET solar and lunar retrievals are conducted at 17 sites for daytime, and 10 sites for nighttime (Fig. 1 and Table 2). The day-night difference analysis is carried out using only sites with more than three years of records of both solar and lunar data at the same day. Six sites are found (blue dots in Fig. 1). Both AERONET solar and lunar data are in Coordinated Universal Time (UTC) and are converted to LST before resampling to IASI observational times to ensure consistency.

2.2.4 LISA

A network of three ground-based observations (Table 2) located on an east–west trajectory of the Sahel and Sahara dust plumes (Sahelian Dust Transect) were deployed in the framework of African Monsoon Multidisciplinary Analysis (AMMA, Redelsperger et al., 2006; Marticorena et al., 2010) international project in 2006. The stations monitor surface PM_{10} (particulate matter with aerodynamic diameter ≤ 10 μm) concentrations, which are mainly dust concentrations, and local meteorological conditions over the Sahel (Marticorena et al., 2010). All the data are maintained by the Laboratoire Interuniversitaire des Systèmes Atmosphériques (Interuniversity Laboratory of Atmospheric Systems; LISA). Hourly observations of LISA PM_{10} concentrations (2008–2020) and surface wind speed and precipitation (2006–2020) are used to understand the day-night differences in dust activities and the potential impacts of meteorological conditions on the day-night differences.

2.2.5 Reanalysis Datasets

We also compare DOD from MERRA-2 (Gelaro et al., 2017; Randles et al., 2017) and EAC4 (Inness et al., 2019) global aerosol reanalysis datasets with IASI DOD. MERRA-2 is the first long-term (1980–present) reanalysis product in which aerosol and meteorological observations are jointly assimilated into global assimilation systems (Gelaro et al., 2017). It assimilates AOD from MODIS onboard Aqua and Terra, MISR, and Advanced Very High Resolution Radiometer (AVHRR) as well as observation from AERONET (Gelaro et al., 2017). EAC4 (Bozzo et al., 2017; Inness et al., 2019) is another aerosol reanalysis product we use in this study. It is produced using 4DVar data assimilation in ECMWF's Integrated Forecast System (IFS), and assimilates remote-sensed AOD from Envisat's AATSR and MODIS from Aqua and Terra (Bozzo et al., 2017). Hourly DOD from MERRA-2 and 3-hourly DOD from EAC4 from 2008 to 2020 are used.

Meteorological variables such as hourly surface winds, vertical velocity at 850 hPa, Convective Available Potential Energy (CAPE), and boundary layer height from ECMWF Reanalysis v5 (ERA5; Hersbach et al., 2020) from 2008 to 2020 are used in this study. Similar variables from MERRA-2 are also used for a comparison. Here, all datasets in UTC were shifted to local time to ensure consistency with IASI. For hourly data, variables at 9:30 a.m. (9:30 p.m.) are approximated by averaging

https://doi.org/10.5194/acp-2022-490
Preprint. Discussion started: 4 October 2022


Atmospheric Chemistry and Physics Discussions

data between 9:00 a.m. and 10:00 a.m. (9:00 p.m. and 10:00 p.m.). A two-tailed t-test is performed at each grid point on the day-night differences in meteorological variables as well as DOD and dust layer height to examine their significance.

2.2.6 IMERG-GPM

Precipitation from the Integrated Multisatellite Retrievals for Global Precipitation Measurements (IMERG; Huffman et al., 2015) is used in this study for the period 2008–2020 to help understand the day-night differences in dust activities over the dust belt. IMERG builds upon the legacy of the Tropical Rainfall Measuring Mission (TRMM) by providing high quality estimates of global rainfall and snow for every 30 minutes at 10 km spatial resolution. The "Final Run" product of IMERG (version V06B), which is calibrated with Global Precipitation Climatology Centre (GPCC) reanalysis product, is used in this study. IMERG has been extensively validated against gauge, gridded, and satellite precipitation products over Africa (Dezfuli et al., 2017; Maranan et al., 2020; Ageet et al., 2022), the Middle East (Hosseini-Moghari and Tang, 2020; Arshad et al., 2021), and Asia (Huang et al., 2018; Kim et al., 2017; Lee et al., 2019). Though the performance of IMERG varies both spatially and temporally, it is shown by these studies to reasonably capture the observed precipitation over the dust belt. Some of the limitations of IMERG include large biases over mountainous areas (Huang et al., 2018), proneness to low-intensity false alarms and overestimation of rainfall amount in weak convective systems over the West African forest zone (Maranan et al., 2020).

2.3 Validate IASI against AERONET station observations

IASI daytime 10 μm DOD has been validated against AERONET solar CAOD by Capelle et al. (2014, 2018) at some selected AERONET sites over land and ocean for 2007–2016. In this work, we extend the initial daytime validation by including nighttime retrievals over the dust belt. Before comparing between IASI and AERONET, it is important to address the differences in their temporal and spatial resolutions as well as spectral bands. First, the sub-hourly AERONET CAOD data in UTC are shifted to LST. We then averaged the station measurements 30 minutes before and after the satellite passage to approximate IASI time. Secondly, we averaged all IASI level 2 pixels falling within a circle of 25 km radius centred at AERONET sites. Lastly, the IASI DOD at 10 μm (IR) is transferred to 500 nm (VIS) by simply determining a site-by-site scale factor of visible (AERONET CAOD) to infrared (IASI DOD) ratio following Capelle et al. (2014, 2018) and Peyridieu et al. (2013) (Table 2). We found a mean IR/VIS ratio of ~0.63 ranging between 0.33 and 1.89 for solar measurements, and ~0.8 ranging between 0.39 and 2.05 for lunar observations. These range of ratios are largely within the range of empirically estimated IR/VIS ratios by Peyridieu et al. (2013) and Capelle et al. (2014, 2018). An accurate conversion requires detailed information about the refractive index, size distribution, and the effective radius of dust particles (Capelle et al., 2014), which are usually not available At the global scale. Thus, the conversion method used in this study may lead to some uncertainties in the magnitude of converted 500 nm IASI DOD.

https://doi.org/10.5194/acp-2022-490
Preprint. Discussion started: 4 October 2022

Atmospheric Chemistry and Physics Discussions

Table 2. AERONET and LISA (italicized and bold) sites used in this study with their location and the short names labelled on figures. Also shown are the ratios of infrared 10 μm DOD to visible CAOD (IR/VIS) for both solar and lunar measurements at each of the AERONET sites. A missing field (dash) means a station has no solar or lunar observations or the station is a LISA site. The sites are divided into North Africa (NA), the Middle East (ME), and Asia (AS) based on their locations.

Site name	Short name	Latitude (°N)	Longitude (°E)	Solar scaling factor (IR/VIS)	Lunar scaling factor (IR/VIS)	Region
Oujda	ouj	34.65	–1.90	0.49	-	NA
Laguna	Lag	28.48	16.32	0.85	-	NA
Dakar	Dak	14.39	–16.96	0.45	0.63	NA
Koforidua	Kof	6.11	–0.30	0.37	0.43	NA
Ilorin	Ilo	8.48	4.68	0.44	0.62	NA
Cinzana	Cin	13.28	–5.93	0.33	-	NA
Zinder Airport	Zai	13.78	8.99	0.63	-	NA
Ben Salem	Bsa	35.55	9.91	0.47	-	NA
Izana	Iza	28.31	–16.50	1.89	2.05	NA
Mezaira	Mez	24.83	53.31	0.46	0.86	ME
Eilat	Eil	29.50	34.92	1.18	-	ME
KAUST Campus	KAU	22.31	39.10	0.45	-	ME
Solar Village	Sol	24.91	46.40	0.34	-	ME
Shagaya Park	Sha	29.21	47.06	-	0.39	ME
Kuwait University	KU	29.33	47.97	-	1.20	ME
Migal	Mig	33.24	35.58	-	0.43	ME
Karachi	Kar	24.95	67.14	0.41	-	AS
Kanpur	Kan	26.51	80.23	0.66	0.72	AS
Jaipur	Jai	26.91	75.81	0.54	-	AS
Lahore	Lah	31.48	74.26	0.73	-	AS
Bhola	Bho	22.23	90.776	-	0.71	AS
Banizoumbou	Ban	13.54	2.66	-	-	NA
M'Bour	Mbo	14.39	-16.96	-	-	NA

https://doi.org/10.5194/acp-2022-490
Preprint. Discussion started: 4 October 2022


Atmospheric Chemistry and Physics Discussions

3. Results

3.1 Evaluation of daytime and nighttime IASI DOD against AERONET CAOD

We evaluate IASI daytime and nighttime DOD against AEORONET ground observations before using the product to understand the day-night differences in dust activities over the dust belt. Figures 2 and 3 show scatter plots of IASI DOD (scaled to 500 nm using the IR/VIS ratios in Table 2) versus AERONET CAOD (500 nm) for daytime and nighttime observations, respectively. Except for Cinzana (Cin) and Zinder Airport (Zai) where AERONET Level 1.5 data are used to increase sample size, all solar sites are evaluated using AERONET Level 2.0 data. Figures 2 and 3 show IASI DOD is highly correlated with AERONET station observations with a statistically significant (95% confidence level) correlation coefficients ranging between 0.36–0.90 for solar sites and 0.47–0.78 for lunar sites. The highest correlation coefficients for solar data are observed in the Saharan and Sahelian dust belt with correlation coefficients up to 0.9 for Oudjda (Ouj) and Cin, followed by the Asian sites, i.e., Karachi (Kar), Kanpur (Kan), Jaipur (Jai), and Lahore (Lah) with correlation coefficients of about 0.89 for all sites (Fig. 2), consistent with similar evaluation in past studies (Peyridieu et al., 2013; Capelle et al., 2014, 2018). The evaluation at some of the Middle East sites i.e., KAUST Campus (KAU) and Solar Village (Sol) yielded high correlations (0.84 to 0.89) and RMSE of 0.16 to 0.22. However, an overestimation of DOD by IASI with a weaker correlation coefficient and higher RMSE is observed at the Eilat (Eil) site (0.36 and 0.16, respectively) possibly due to its closeness to the coast where sea salt aerosols can be mixed with dust aerosols and the complicated land surface conditions in the area leading to difficulties in DOD retrieval (Capelle et al., 2014, 2018). The average correlation coefficient is about 0.81 for North African sites, 0.67 for the Middle East, and 0.87 for the South Asian sites.

https://doi.org/10.5194/acp-2022-490
Preprint. Discussion started: 4 October 2022

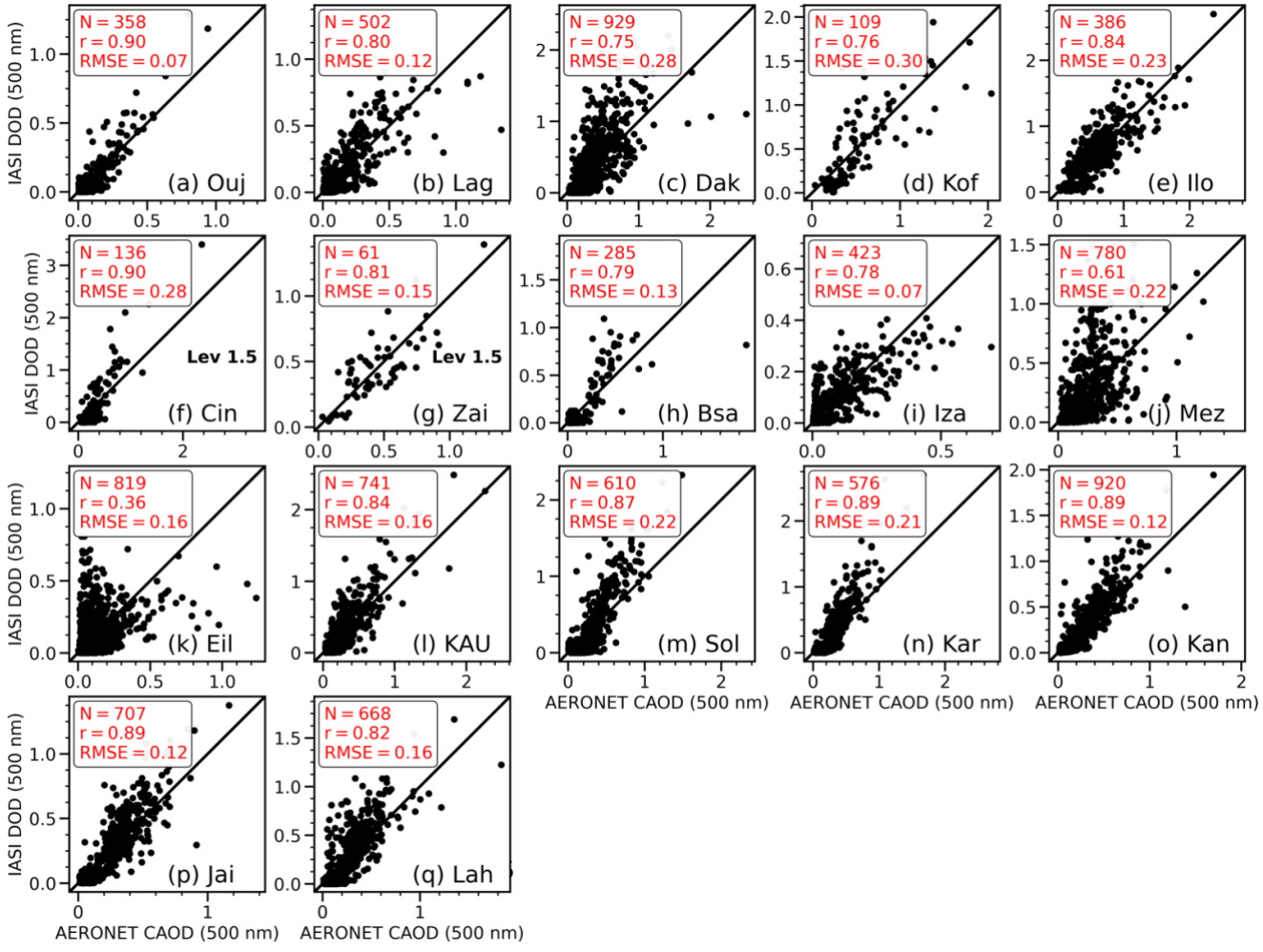

Figure 2: Scatterplots of daytime IASI DOD versus AERONET CAOD over 17 AERONET solar sites across the dust belt (see locations in Fig. 1). *r* is the correlation coefficient between IASI DOD and AERONET CAOD, *RMSE* is the root mean square error, and *N* is the sample size of data at each site. The IASI DOD at 10 μm is scaled to 500 nm equivalence using an IR/VIS ratio estimated from each AERONET site (Table 2). AERONET CAOD was sampled between 9:00 a.m. and 10:00 a.m. to compare with daytime IASI DOD at 9:30 a.m. Note that level 2 AERONET CAOD data are used for all sites except in (f) and (g) where only level 1.5 data are available. IASI DOD was sampled around each AERONET site within an approximate radius of 25 km.

The correlations over lunar sites are generally lower than solar sites (Fig. 3). While over sites like Kan and Dak where correlations between IASI DOD and AERNOET CAOD are higher than 0.7, correlations over other sites are around 0.51~0.64, with the lowest correlation of 0.47 at Mezaira (Mez) site. Note that the correlation coefficient of solar CAOD at Mez site (~0.61) is also at the lower end of correlations among available sites (Fig. 2). This discrepancy between IASI DOD and AERONET CAOD daytime records at Mez site is also noticed by Capelle et al. (2008) who attributed the lower correlation partially to the

https://doi.org/10.5194/acp-2022-490
Preprint. Discussion started: 4 October 2022

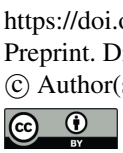

Atmospheric Chemistry and Physics Discussions

heterogeneity of land surface or rapid varying near-surface dust plume that may reduce the sensitivity of infrared sounders. Reasons for the lower correlation in lunar data could range from smaller sample size of lunar data to the quality of lunar data used in the evaluation, which are cloud screened but not quality assured. Overall, 94% of the solar sites analyzed have correlations above 0.6 whereas 50% of the lunar sites analyzed in this work have correlation coefficients above 0.6. In general, IASI DOD at sites closer to dust sources is better correlated with AERONET CAOD than sites far from dust sources.

In addition to these scatter diagrams, an examination of the seasonal cycle of IASI DOD and AERONET CAOD show IASI accurately captures the seasonal variability of dust events as depicted by AERONET ground-based observations in the dust belt (Figs. S1 and S2 in the Supplement). These results indicate that IASI shows quality performance in capturing the spatiotemporal distribution of dust aerosols over the dust belt can therefore be used to understand the day-night differences in dust activities.

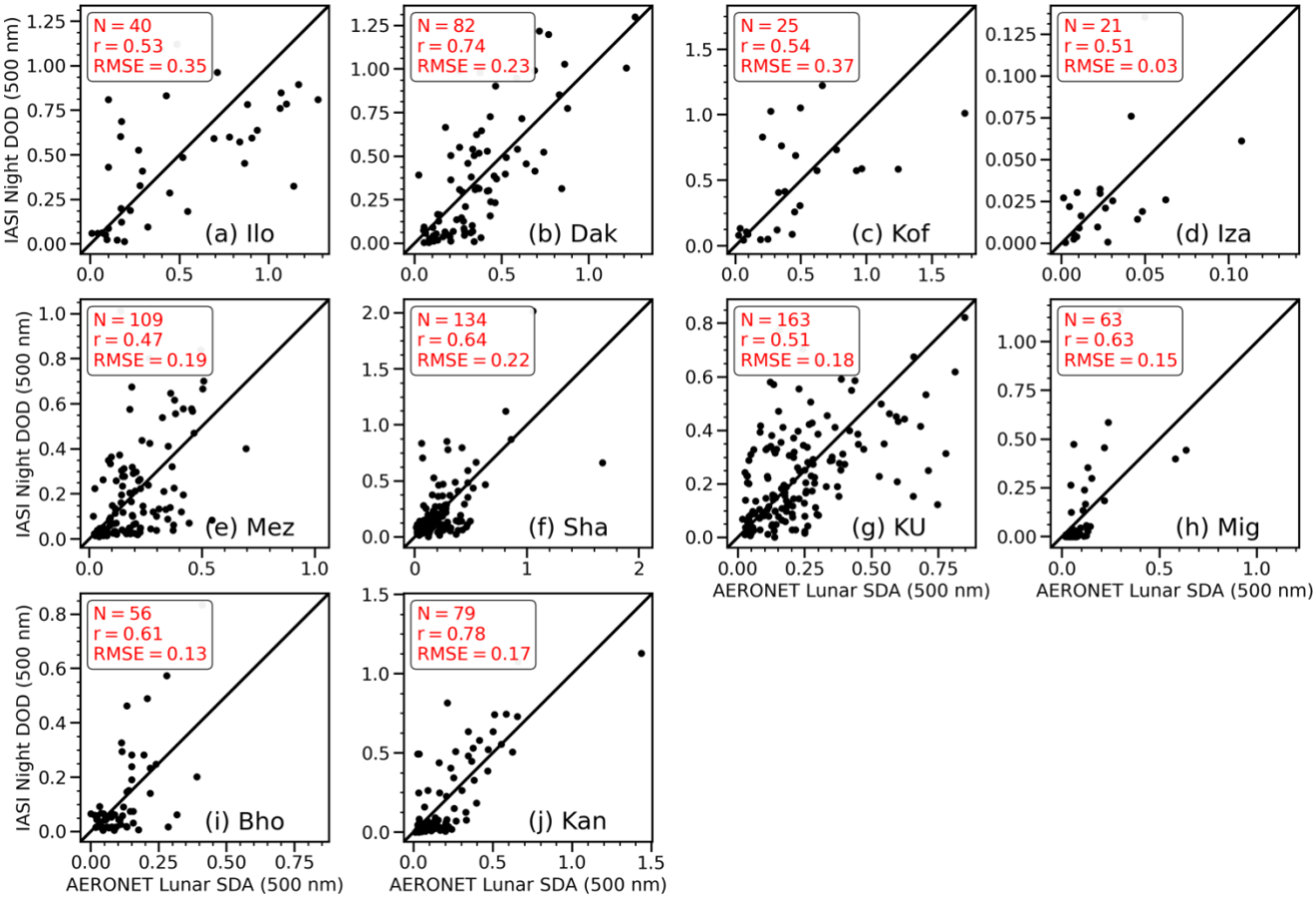

Figure 3: Same as Fig. 2. but compares nighttime (9:30 p.m.) IASI DOD with AERONET CAOD at 10 lunar sites. AERONET CAOD was sampled between 9:00 p.m. and 10:00 p.m.

https://doi.org/10.5194/acp-2022-490
Preprint. Discussion started: 4 October 2022


Atmospheric Chemistry and Physics Discussions

3.2 Characteristics of daytime and nighttime dust activities over the dust belt

In this section, we examine the characteristics and differences between daytime (9:30 a.m.) and nighttime (9:30 p.m.) DOD and dust layer height from IASI, along with CAOD from selected six AERONET stations and surface PM_{10} concentrations from LISA sites. Figure 4 shows the annual and seasonal mean climatology (2008 to 2020) of IASI DOD, AERONET CAOD (scaled to 10 μm), and surface PM_{10} concentration for daytime, nighttime, and day-night difference. Both daytime and nighttime DOD show similar seasonal cycles. In winter (DJF), the dustiest regions occur in the southern parts of the Sahel to the Guinea Coast (Fig. 4b, g). By spring (MAM), the maximum DOD begins to transition more northward from the Sahel and the Guinea Coast towards the central to northern parts of the Sahara (Fig. 4c, h) and maximizes around summer (JJA) in the central towards the northwestern Sahara (Fig. 4d, i). At the same period, a pronounced DOD maximum is observed in the central parts of the Arabian Peninsula, northwestern parts of the Indian Subcontinent, around the Iraqi and Irani deserts, and the Taklamakan Desert in northwestern China. DOD reduces in fall (SON), with a magnitude comparable to that in DJF over the Middle East and Asia, but slightly stronger over the Sahara Desert yet weaker over the Sahel (Fig. 4e, j). Such seasonal migration of dust maxima is largely driven by the meridional shift of the Intertropical Convergence Zone (ITCZ) and generally consistent with previous studies about dust activities in this region via satellite retrievals (e.g., Ginoux et al., 2012; Pu and Ginoux, 2018; Yu et al., 2019; Chédin et al., 2020; Vandenbussche et al., 2020; Yu et al., 2021; Li et al., 2021).

Figure 4 also demonstrates statistically significant (95% confidence level) differences between daytime and nighttime DOD. The day-night differences in DOD, i.e., daytime minus nighttime, are positive over dust source regions (i.e., most parts of the Sahara, the central Arabian Peninsula, parts of South Asia around East Iran, southwest Afghanistan, and central Pakistan, and the Taklamakan Desert) yet negative over regions close to dust sources (i.e., the southern Sahel to the Guinea Coast, the south coast of the Arabian Peninsula, and India). It is also important to note that there is a seasonal variability of the magnitude of the day-night differences in DOD, with the largest magnitude of the day-night difference in DOD in DJF and MAM (Fig. 4l, m) and a weaker magnitude in JJA and SON (Fig. 4n, o). The spatial pattern of the day-night differences in DOD in JJA is consistent with the day-night difference in dust emissions over North African dust sources shown by Chédin et al. (2020; e.g., their Fig. 4) and Todd and Cavazos-Guerra (2016; e.g., their Fig. 8).

https://doi.org/10.5194/acp-2022-490
Preprint. Discussion started: 4 October 2022

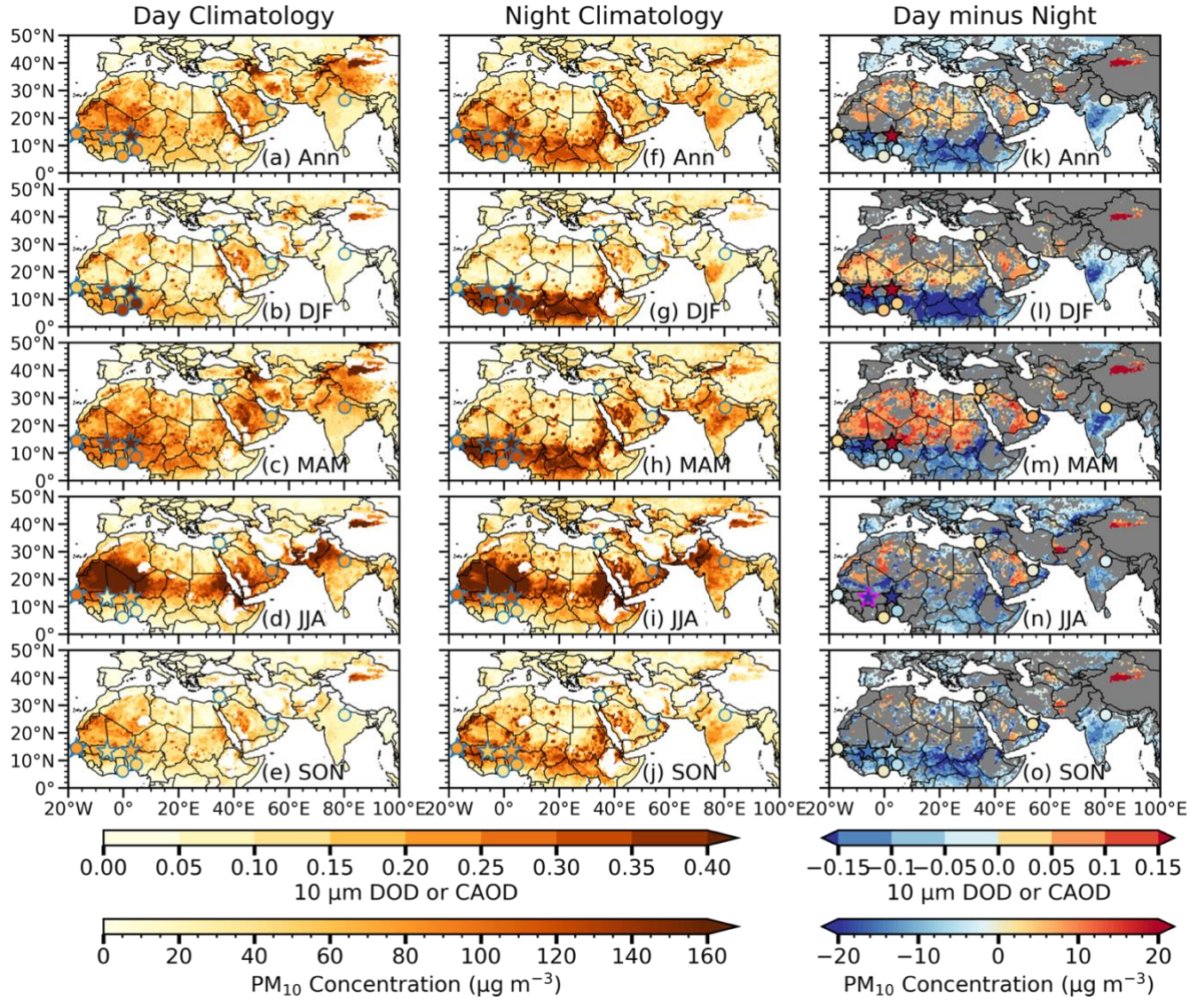

Figure 4: Annual (Ann) and seasonal means of IASI DOD from 2008 to 2020 at (a)–(e) daytime (9:30 a.m.), (f)–(j) nighttime (9:30 p.m.), and (k–o) day-night differences, along with LISA PM_{10} concentrations averaged over 2008–2020 and AERONET CAOD scaled to 10 µm (using an IR/VIS ratio of 0.63) overlayed as stars and dots, respectively. The white color denotes oceanic grid cells and missing values over land. The grey color in (k–o) show grid cells where day-night differences in DOD do not pass the 95% confidence level (t-test). The magenta color around the edges of LISA and AERONET sites in the difference plots show sites where the day-night differences in CAOD or PM_{10} concentrations pass the 95% confidence level.

Surface observations of dust properties are also examined to compare with results from IASI products. Here a uniform scaling factor, 0.63, by averaging all IR/VIS ratios in Table 2, are used to convert both daytime and nighttime AERONET CAOD to 10 µm. Using individual ratios will slightly improve the consistency between AERONET CAOD and IASI DOD

https://doi.org/10.5194/acp-2022-490
Preprint. Discussion started: 4 October 2022


Atmospheric Chemistry and Physics Discussions

(not shown) but may lead to some biases in the day-night differences. AERONET CAOD overlayed as circles on the IASI DOD show the two datasets generally agree on the seasonal daytime and nighttime distributions of dust aerosols (Fig. 4a–j). For instance, the day-night differences in CAOD for sites in the Guinea Coast (Kof and Ilo) are also negative in MAM (Fig. 4m), and in JJA and SON for Ilo site (Fig. 4n, o). The Sahel site (Dak) is consistent with IASI in JJA (Fig. 4n) with a negative day-night difference in CAOD, while the site at the Indian subcontinent (Kan) has a negative difference in all seasons except MAM (Fig. 4l, m, n, o). The magnitude and sign of the day-night difference in AERONET CAOD are largely consistent with IASI DOD in the Arabian Peninsula sites as well. Note that unlike IASI, the day-night differences in CAOD are insignificant over all sites and seasons in AEROENT, likely due to smaller sample sizes and the lower quality of AERONET lunar data (level 1.5, cloud screened but not quality assured) in comparison with solar data (mostly level 2). The inconsistency between IASI and AERONET may be partially due to the uncertainties of using CAOD to approximate DOD and uncertainties in IASI retrieval (see discussion in section 3.7) as well.

Surface observations of PM_{10} concentrations at both daytime and nighttime from LISA are also overlayed as stars on the IASI DOD in Fig. 4. The seasonal cycle of surface PM_{10} concentration is similar to IASI DOD over the Sahel, with larger values in DJF and MAM yet smaller values in JJA and SON when monsoon precipitation greatly reduces surface dust concentrations by wet scavenging (Marticorena et al., 2010). Negative day-night differences in PM_{10} are seen all year long at Mbo site over the west coast of the Sahel, which is largely consistent with the sign of IASI DOD but opposite to AERONET CAOD at Dak. Positive day-night differences in PM_{10} concentrations are seen in DJF at Ban and Cin sites and in MAM at Ban site, but negative in other seasons (Fig. 4l-o), somewhat similar to the patterns of IASI DOD. In JJA, a significantly negative day-night difference in PM_{10} concentrations is found at the Cin site, again consistent with the sign of the day-night differences in IASI DOD (Fig. 4n). Although DOD and surface PM_{10} concentrations reveal different aspect of dust activities, these results demonstrate that the day-night differences in surface PM_{10} concentration is generally consistent with the day-night differences in DOD over the Sahel dust belt.

IASI also retrieves dust layer height, a variable that can be useful in characterizing the day-night difference in dust activities. Figure 5 shows the annual and seasonal mean climatology of daytime, nighttime, and day-night differences in dust layer height. The dust layer height reaches about 2.4–3.6 km in dust source regions over the Sahara Desert and the Sahel, the central Arabian Peninsula, and the deserts in Central and East Asia in the annual mean (Fig. 5a, f), and are generally higher in DJF and MAM seasons (Fig. 5b, c, g, h) and lower in JJA and SON (Fig. 5e, j). The lower summertime dust layer height is somewhat in contrast to previous studies using CALIOP (e.g., Yu et al., 2010; Clarisse et al., 2019; See Fig. S4 and more discussion below). Negative day-night differences in dust layer height, i.e., lower dust layer height at 9:30 a.m. than 9:30 p.m., are observed mainly in dust source regions (e.g., large parts of the Sahara Desert, Arabian Peninsula, and the Taklamakan Desert), while positive differences are found over the dust downwind regions (e.g., the southern Sahel to the Guinea Coast and large areas in the Indian subcontinent (Fig. 5k–o). The magnitude of the day-night differences in dust layer height shows little seasonal variations. Overall, dust layer height are lower over major dust source regions in daytime than in nighttime, largely

https://doi.org/10.5194/acp-2022-490
Preprint. Discussion started: 4 October 2022

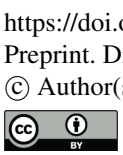

Atmospheric Chemistry and Physics Discussions

opposite to that of IASI DOD, and generally consistent with the dust emission index defined by Chédin et al. (2020) that shows higher DOD and lower dust layer height in dust source regions.

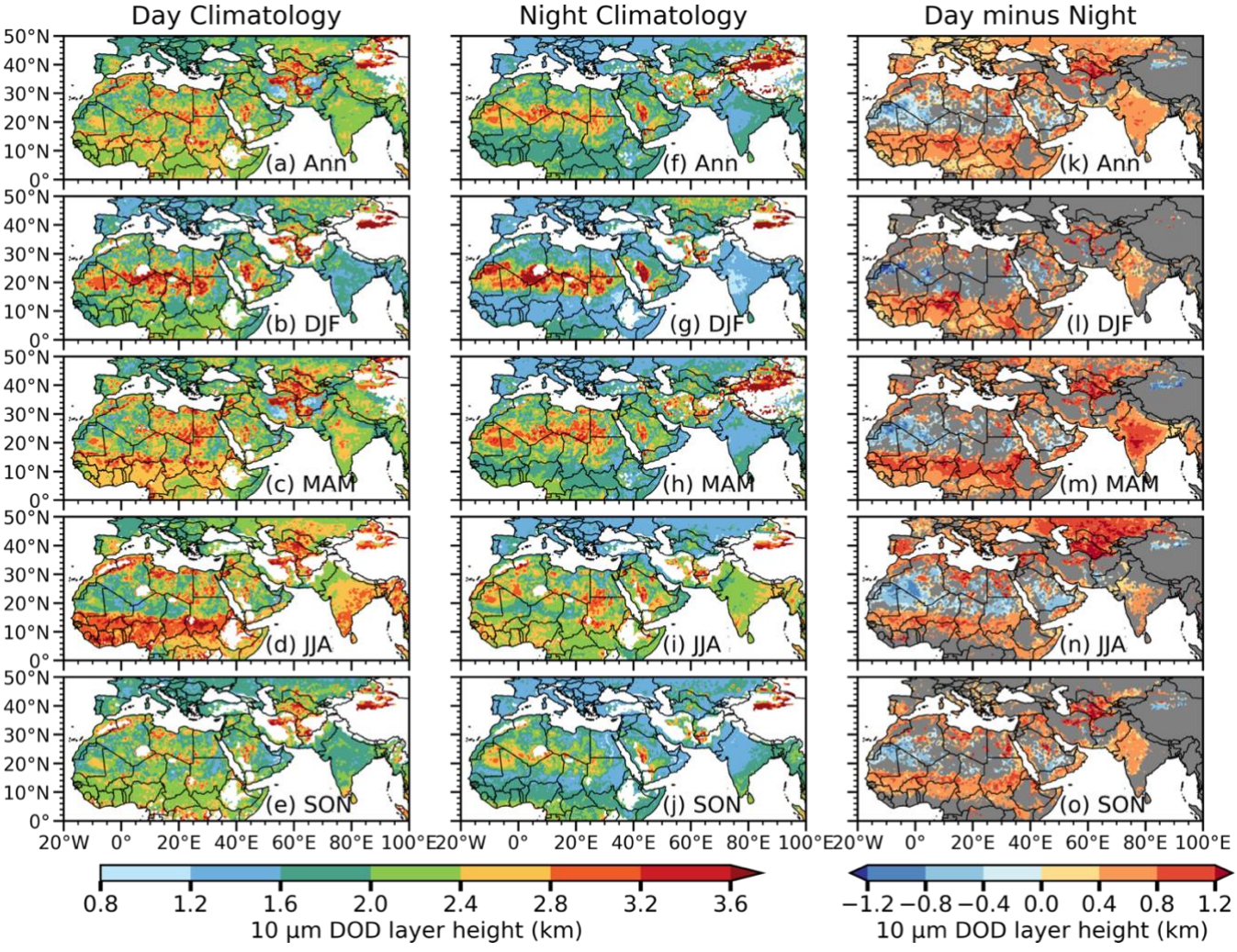

Figure 5: Same as Fig. 4., but for dust layer height (km) from IASI. Dust layer height is defined as the height where half of the vertically integrated DOD is above, and the other half is below.

The seasonal cycle of daytime (1:30 p.m.) and night (1:30 a.m.) DOD and dust layer height from CALIOP is also investigated to compare with IASI data (Figs. S3 and S4, respectively). The seasonal cycle of CALIOP DOD is very similar to IASI, consistent with the finding of Yu et al. (2019), although IASI shows a larger area of high DOD over the Guinea coast at nighttime in DJF (Figs. 4g, S3g). The day-night differences in DOD from CALIOP are insignificant for most parts of the dust belt across all the seasons except for narrow regions of the northern Sahara and parts of central Asia and western China in MAM, JJA and SON and are in generally opposite to IASI, except along the Mediterranean coast. Such an inconsistency in

https://doi.org/10.5194/acp-2022-490
Preprint. Discussion started: 4 October 2022


Atmospheric Chemistry and Physics Discussions

day-night differences of DOD between IASI and CALIOP may be partially related to low signal-to-noise ratio of CALIOP daytime data and different overpassing times of two instruments.

In contrast with IASI, dust layer height in CALIOP shows maximum altitude in JJA over major dust source regions and minimum in DJF (Fig. S4). Previous studies show IASI dust layer height is systematically biased low by about –0.4 km in comparison with CALIOP (Peyridieu et al., 2013; Capelle et al., 2014), however, here we found that the maximum altitudes are comparable between the two datasets over North Africa. The afternoon (1:30 p.m.) and midnight (1:30 a.m.) dust layer height from CALIOP is also not significantly different from each other in most part of the dust belt, except around the southern Sahel to the Guinea Coast, southern Arabian Peninsula, and parts of the western Taklamakan Desert in DJF, western China in MAM, northern and eastern Sahara and part of central Asia in JJA, and western China in SON (Fig. S4l–o), while sharing some similarity with IASI over the western Taklamakan Desert, central Asia (JJA), and coastal northwestern Africa (JJA). The differences between IASI and CALIOP dust layer height could be attributed to several factors (Peyridieu et al., 2013; Chédin et al., 2020), such as different definitions of dust layer height, e.g., arithmetic mean dust layer height in CALIOP versus cumulative extinction height in IASI, and different overpass times of the two instruments (CALIOP lags IASI in about 4 hours). Kylling et al. (2018) found that the bias of dust layer height in IASI (LMD version) would be lower if CALIOP dust layer height was defined by cumulative extinction height instead of arithmetic mean and was shifted to the observation time of IASI.

3.3 Seasonal cycle of day-night dust activities from IASI, LISA, and AERONET

We compare the seasonal cycle of daytime and nighttime IASI DOD with LISA and AERONET ground-based observations to better understand how day-night differences in dust activities propagate in seasons. Figure 6 shows monthly mean surface PM_{10} concentrations from three LISA sites (Ban, Cin and Mbo; see locations in Fig. 1) and monthly mean DOD from IASI averaged over ±0.5° around LISA sites. We average hourly PM_{10} concentrations between 9 a.m. and 10 a.m. (9 p.m. and 10 p.m.) to approximate values at 9:30 a.m. (9:30 p.m.) for a consistent comparison with IASI. Note that the seasonal cycle of LISA records is different from DOD, with a minimum in JJA associated with monsoon rainfall and a peak in DJF and MAM due to transported dust from the central Sahara (Marticorena et al., 2010). Daytime PM_{10} concentrations are significantly higher than nighttime PM_{10} concentrations in DJF and early MAM at three LISA sites along 13–14° N in the Sahel, while nighttime dust concentrations are higher than daytime from late MAM to early SON (early JJA) at Ban and Cin (Mbo; Fig. 6a-c). Like LISA PM_{10}, daytime IASI DOD is higher than nighttime in most of DJF and MAM months but lower in JJA and SON, consistent with the results shown in Fig. 4. Note that different from PM_{10} concentrations, nighttime IASI DOD at Mbo is higher than daytime from late SON to DJF. This disparity could be due to the influence of sea salt on PM_{10} records as Mbo site is on the west coast, near the North Atlantic.

https://doi.org/10.5194/acp-2022-490
Preprint. Discussion started: 4 October 2022

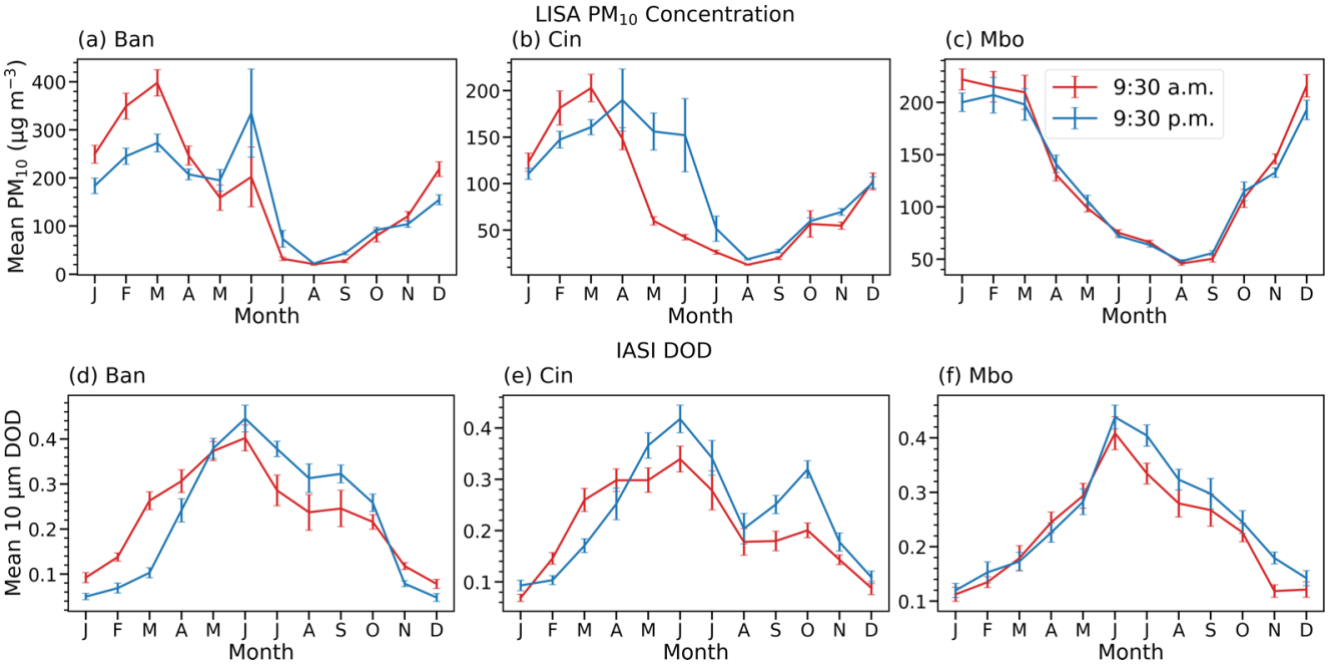

Figure 6: Seasonal cycle of (a)–(c) PM_{10} concentrations (µg m^{-3}) from LISA sites and (d)–(f) DOD from IASI at the same locations averaged from 2008 to 2020 except for LISA PM_{10} in Mbo where the average is from 2008-2019. The error bars show standard errors. PM_{10} concentrations are averaged between 9:00 am and 10:00 am (9:00 pm and 10:00 pm) to get values at 9:30 am (9:30 pm).

Similar analysis is conducted over six AERONET sites (blue dots in Fig. 1) and IASI as shown in Fig. 7. AERONET CAOD at 9:30 a.m. and 9:30 p.m. are used. CAOD and IASI DOD show very similar seasonal cycles, with maxima in the late MAM to JJA for stations in the Sahara (Dak), Middle East (Mez and Mig) and Asia (Kan), whereas the Guinea coast stations (Ilo and Kof) showed maximum DOD or CAOD in late DJF to MAM. AERONET nighttime CAOD is higher than daytime for the sites in the Guinea Coast most time of the year, which is consistent with IASI. While seasonal variations in day-night differences in CAOD are largely similar to IASI DOD at Ilo, Kof, discrepancies are found at Mez in JJA and SON, Mig in MAM, and Kan in MAM and JJA, probably in association with the relatively smaller sample size and lower quality (level 1.5) of AERONET lunar data and impacts of sea salt on CAOD at coastal stations.

https://doi.org/10.5194/acp-2022-490
Preprint. Discussion started: 4 October 2022

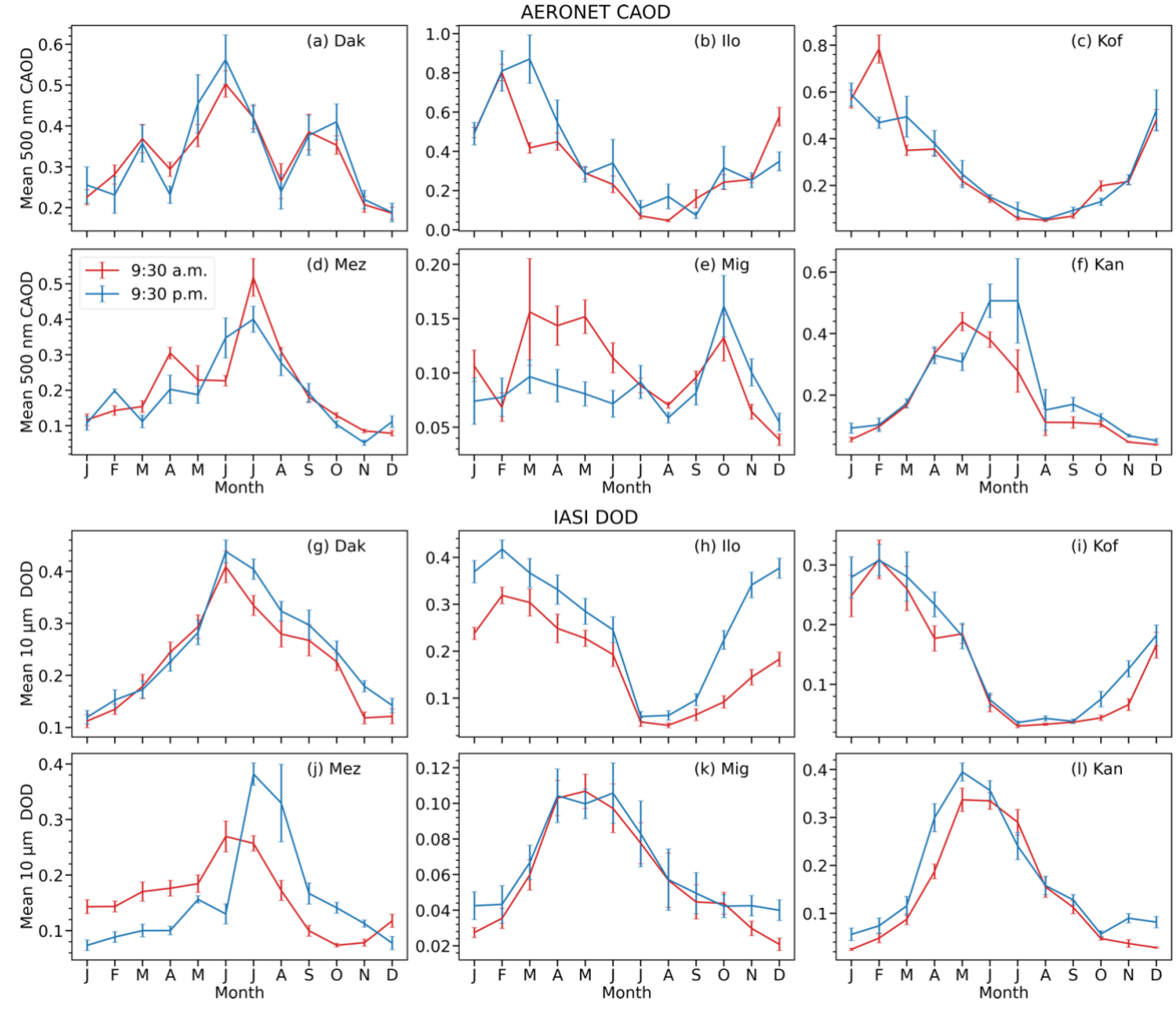

Figure 7: Seasonal cycle of (a)–(f) AERONET CAOD at 500 nm and (g–l) IASI DOD at 10 µm at the same locations. The seasonal cycle of IASI DOD was computed for a temporal range between 2008 and 2020 whereas the temporal range of AERONET varies from site to site but within 2008 to 2020. AERONET solar and lunar observations are sampled between 9:00 a.m. and 10:00 a.m. (9:00 p.m. and 10:00 p.m.) to approximate 9:30 a.m. (9:30 p.m.) of IASI.

3.4 Diurnal variations in dust activities

IASI DOD and dust layer height are available only two times daily. To have a clear picture of the full diurnal cycle of dust activities, data with higher temporal resolution are required. Here we use station data, i.e., typically five to 15 minutes

https://doi.org/10.5194/acp-2022-490
Preprint. Discussion started: 4 October 2022

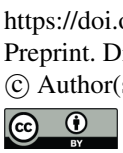

Atmospheric Chemistry and Physics Discussions

AERONET CAOD and hourly LISA PM_{10} concentrations, to further explore diurnal variations in dust over the dust belt. Figure 8 represent the diurnal cycle of surface PM_{10} concentration in the Sahel (first row) and CAOD at AERONET sites (last two rows) for each season, with cyan vertical lines highlighting the overpassing time of IASI. The results indicate that surface PM_{10} concentrations at the three LISA sites in the Sahelian dust belt peak around 9 a.m.–11 a.m. LST in the late morning in all seasons, except JJA, when PM_{10} concentrations are low due to precipitation scavenging. Both Cin and Mbo sites have evening peaks around 7–8 p.m. LST (except JJA at Mbo; Fig. 8b, c), but not very evident at Ban site, which shows a peak around mid-night in MAM (Fig. 8a). The passing time of IASI is largely consistent with the peaks of surface PM_{10} concentrations, with the 9:30 a.m. passing time slightly ahead of the late morning peak and while the 9:30 p.m. passing time slightly behind the second peak in the evening.

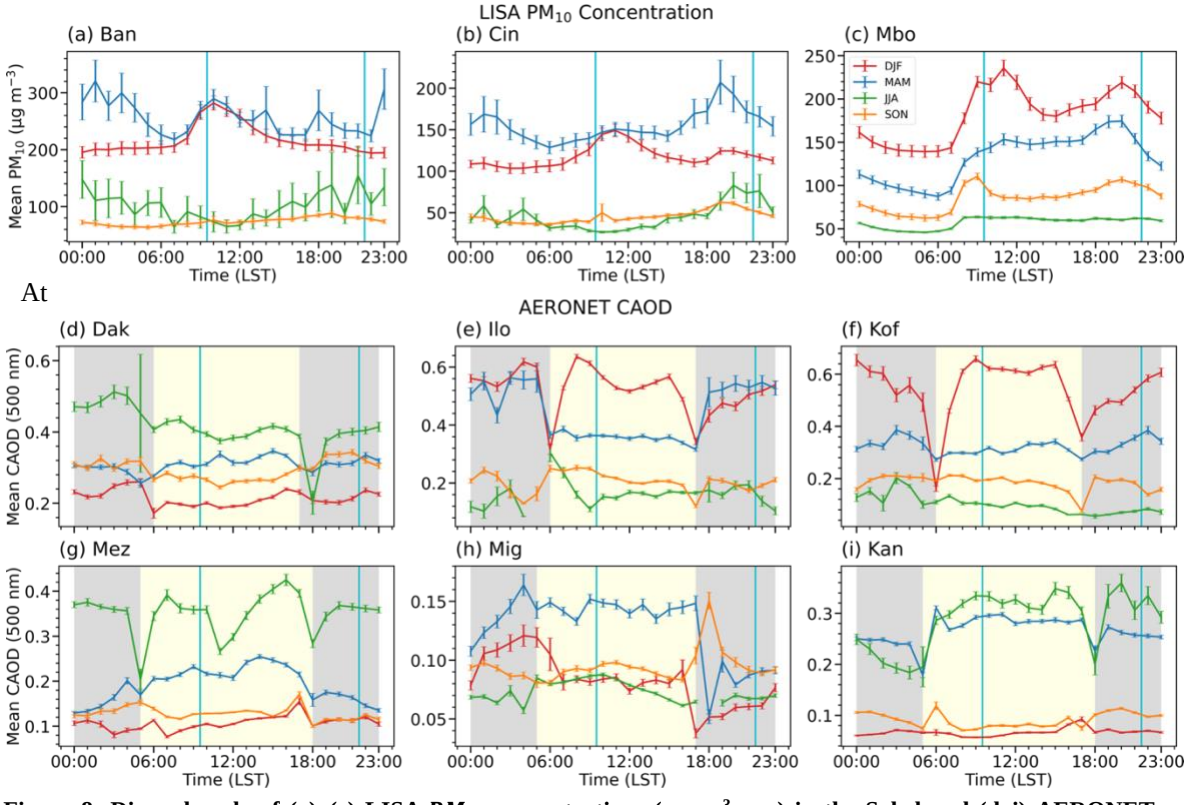

Figure 8: Diurnal cycle of (a)–(c) LISA PM_{10} concentrations (μg m^{-3}, a–c) in the Sahel and (d–i) AERONET CAOD over sites across the dust belt. The diurnal cycle of LISA PM_{10} concentrations were averaged between 2008 and 2020 for Ban and Cin sites, and between 2008 and 2019 for Mbo site. The temporal ranges for AERONET data vary depending on the number of records available for both solar and lunar datasets. The cyan lines mark 9:30 a.m. and 9:30 p.m. LST. The grey (light yellow) background shading shows the temporal range of lunar (solar) observations. Error bars show standard errors.

At AERONET sites, daytime records (6 a.m. to 5 p.m. for Dak, Ilo, and Kof sites; 5 a.m. to 6 p.m. for Mez, Mig, and Kan; light yellow shading in Fig. 8) are observed by sun photometer, and nighttime data (6 p.m. to 5 a.m. for Dak, Ilo, and Kof; 5 p.m. to 6 a.m. for Mez, Kan; 5 p.m. to 5 a.m. for Mig; grey shading in Fig. 8) are from lunar photometer, thus the discontinuity between

https://doi.org/10.5194/acp-2022-490
Preprint. Discussion started: 4 October 2022


Atmospheric Chemistry and Physics Discussions

daytime and nighttime records is likely due to different instruments (Fig. 8d–i). Furthermore, level 1.5 lunar data also have higher uncertainty compared to level 2.0 solar data. AERONET CAOD also peaks in the morning around 7–9 a.m. LST for sites in the Guinea Coast (Ilo and Kof), the Sahel (Dak), the Middle East (Mez), and the Indian subcontinent (Kan) which is consistent with previous work in this region (Schepanski et al., 2009; Marticorena et al., 2010; Kaly et al., 2015; Yu et al., 2019; Yu et al., 2021). A secondary peak of CAOD occurs in the afternoon around 3 p.m. LST (e.g., at Dak, Ilo, Kof, Mez, and Kan sites; Fig. 8d, e, f, g, i). The nighttime peak of CAOD varies in different regions. In North Africa, CAOD maximizes around 3 a.m. in Dak, 4 a.m. in Ilo, and midnight in Kof, while in the Arabian Peninsula CAOD peaks around 5 a.m. in Mig site but without a clear peak in Mez site (slightly higher around 8 p.m. and 1 a.m. in JJA; Fig. 8d–h). At Kan site in the Indian subcontinent, an evening peak at about 8 p.m. is found (Fig. 8i). Overall, the available AERONET data in the dust belt show that IASI 9:30 a.m. data largely captures the early morning peak of CAOD, while the 9:30 p.m. data partially capture the increasing CAOD before their nighttime maxima. As revealed by LISA and AERONET station data, dust activities at 9:30 a.m. and 9:30 p.m. could be quite different or similar to each other depending on the location of the site. Although IASI data only contains two-time steps, its high spatial resolution and global coverage provide useful information that complements sparsely located ground observations to help understand the diurnal cycle of dust.

3.5 Daytime and nighttime dust optical depth from reanalysis products

With global coverage and high temporal resolution, aerosol products from reanalysis will offer great tools to study diurnal cycle of dust if they largely capture the observed day-night dust variations shown in satellite retrievals. Here we examine daytime and nighttime DOD from MERRA-2 and EAC4 to examine whether they capture the day-night differences in DOD as revealed by IASI in the dust belt. After the reanalysis datasets are shifted from UTC to LST for consistency with satellite observations as discussed in section 2.2.5, the annual and seasonal climatology of daytime (9:30 a.m.), nighttime (9:30 p.m.), and day-night differences in DOD from MERRA-2 and EAC4 are presented in Figs. 9 and 10, respectively. Like IASI, the results of the seasonal mean climatology of MERRA-2 and EAC4 DOD from 2008 to 2020 also revealed a higher DOD in MAM and JJA in comparison with other seasons. The magnitude of the day-night difference in DOD is however very weak in the reanalysis products and largely insignificant as compared to that of IASI (Figs 9. And 10). The magnitude of the day-night difference in MERRA-2 DOD appears to be large only in the Bodélé depression (centered around 17°N, 18°E), with a positive difference throughout the year and a negative difference to the northwest (Fig. 9l-o). Over northeastern Africa and coastal area of the Arabian Peninsula and central Asia, some areas also show significant negative differences, i.e., with greater nighttime DOD. The sign of the day-night differences in MERRA-2 DOD is largely consistent with IASI at parts of the Bodélé depression and southern Arabian Peninsula in DJF and MAM and central Asia in JJA but not in other regions or season.

https://doi.org/10.5194/acp-2022-490
Preprint. Discussion started: 4 October 2022

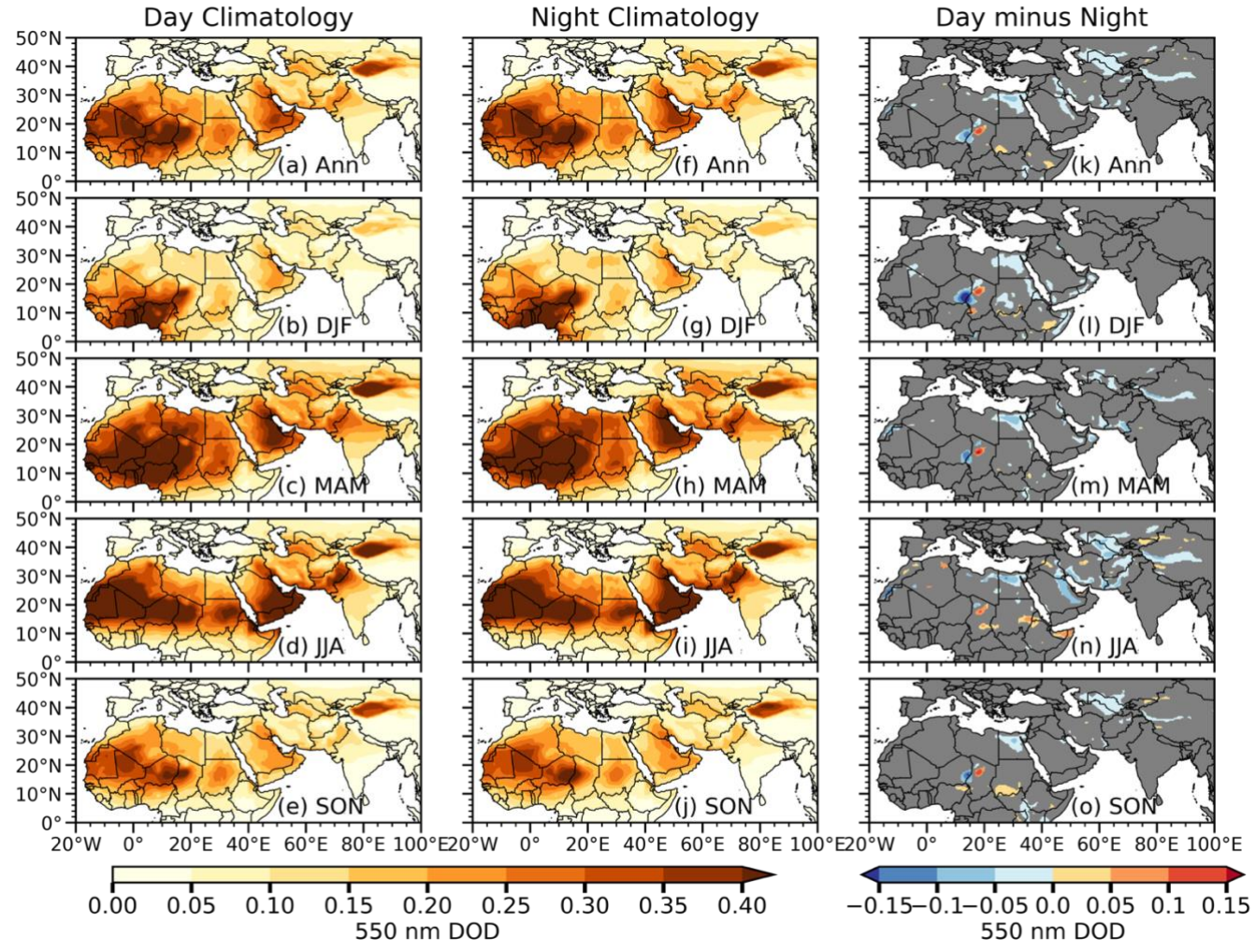

Figure 9: Annual (Ann) and seasonal means of MERRA-2 DOD averaged between 2008 and 2020 (a)–(e) at daytime (9:30 a.m.), (f)–(j) nighttime (9:30 p.m.), and (k)–(o) day-night differences (k–o). Areas where day-night differences in DOD do not pass the 95% confidence level (t-test) in (k–o) are masked out in grey.

A slightly larger portion of the central to northern Sahara, the Middle East, central Asia, and the eastern Taklamakan Desert are characterized by significant and negative day-night differences in DOD in EAC4 (Fig. 10l-o). In most of these areas, the day-night differences are opposite to that of IASI, except over southern Arabian Peninsula and in northwest Sudan and central Asia in JJA. As shown in Figs. 9 and 10, aerosol reanalyses in general have difficulties in capturing the day-night differences in DOD shown by IASI. This may be partially because reanalyses do not assimilate nighttime observations (e.g., AERONET lunar data or infrared satellite products) to constrain AOD or DOD.

https://doi.org/10.5194/acp-2022-490
Preprint. Discussion started: 4 October 2022

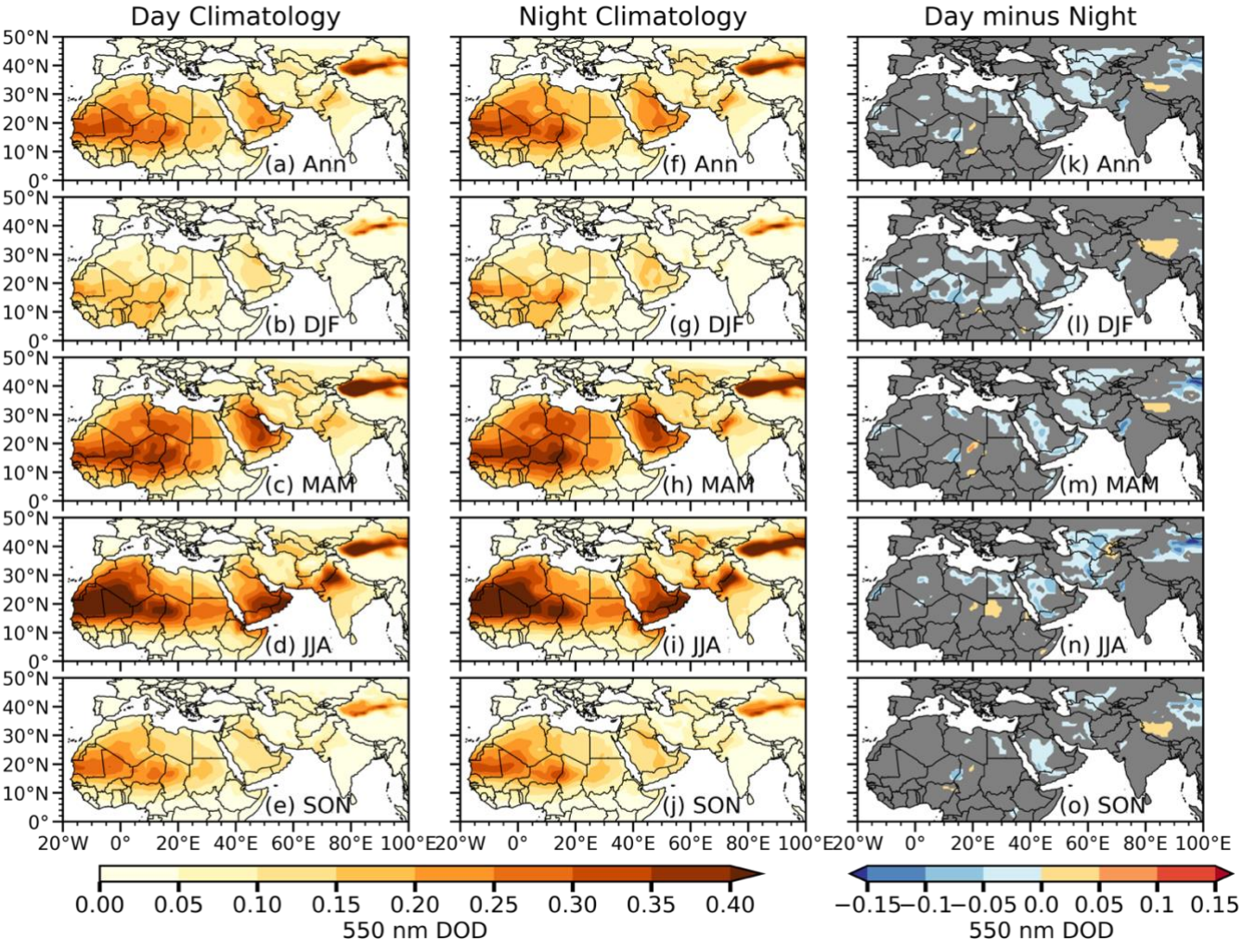

Figure 10: Same as Fig. 9., but for EAC4.

3.6 Meteorological factors contributing to the observed day-night differences in dust activities

In this section we examine the impacts of meteorological conditions on the daytime and nighttime dust activities, mainly DOD and dust layer height from IASI, over the dust belt using meteorological variables from MERRA-2, ERA5, IMERG, and LISA observational datasets.

https://doi.org/10.5194/acp-2022-490
Preprint. Discussion started: 4 October 2022

Atmospheric Chemistry and Physics Discussions

3.6.1 Near-surface winds

Wind speed of appreciable magnitude can enhance dust emissions over dust source regions (Fernandez-Partagas et al., 1986; Todd et al., 2008; Schepanski et al., 2009; Marsham et al., 2011; Fiedler et al., 2013). To understand the impact of surface winds on the daytime and nighttime variations in dust activities, Fig. 11 show the annual and seasonal mean climatology of daytime, nighttime, and day-night difference in surface wind speed from ERA5. Daytime wind speed is strong in magnitude and mostly northeasterly over the large area of North Africa in DJF, MAM, and SON (Fig. 11b, c, e) with a maximum in DJF over the central Sahara around the Bodélé Depression in Chad. These results are consistent with the findings of Fiedler et al. (2013) and Schepanski et al. (2009) which showed a high frequency of nocturnal low-level jets over the Bodélé Depression in DJF . Surface winds also maximize in northwestern China near the Taklamakan Desert in DJF. The strong surface winds over dust source regions, such as the Sahara Desert and the Bodélé Depression, not only favor local dust emissions but also transport dust toward downwind areas, e.g., the Guinean coast (Figs. 4b, c, e). During JJA, following the development of the West African monsoon and Indian summer monsoon, surface winds become southwesterly over the Sahel and the Guinea Coast and over large parts of the Indian subcontinent (Fig. 11d, i). Consequently, high magnitude of DOD is largely located over the northern Sahel and southern central Sahara between 15 °N and 30 °N in North Africa and central to northern Pakistan in summer (Fig. 4d).

Nighttime wind speeds are slightly weaker in comparison to the daytime (Fig. 11f–j). The magnitude of day-night difference in surface wind is relatively strong during DJF–JJA, with a maximum in JJA (Figs. 11l–o). In North Africa, the day-night difference in surface wind speed is positive, i.e., with stronger daytime winds, and significant everywhere except over the northern portion of the Sahara along the coast of the Mediterranean Sea where the differences remain negative for all seasons and over the Guinea coast where the differences are negative in DJF, MAM, and SON (Fig. 11l–o). Daytime surface wind speeds are more than 2 m s^{-1} higher than nighttime winds in some areas over the Sahara Desert, likely resulting in stronger dust emissions and higher DOD in the Sahara during daytime. The weaker daytime winds over the central Arabian Peninsula and the Taklamakan Desert indicate that day-night difference in surface winds cannot explain higher daytime DOD in these source regions. Surface wind speed from MERRA-2 (Fig. S5) revealed similar results except that the day-night differences in surface winds are the strongest in DJF in MERRA-2 (Fig. S5).

https://doi.org/10.5194/acp-2022-490
Preprint. Discussion started: 4 October 2022

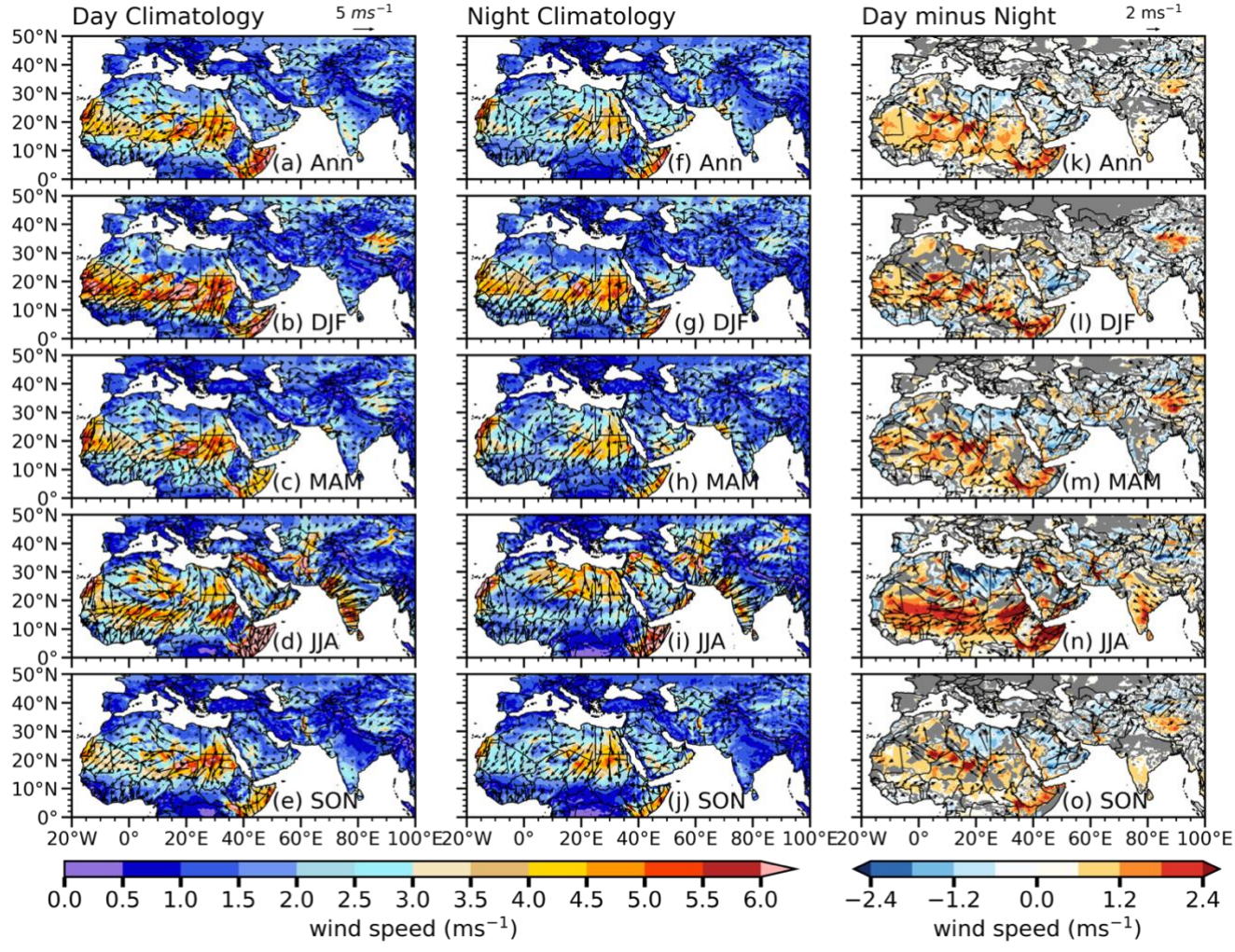

Figure 11: Annual (Ann) and seasonal mean surface winds climatology (2008–2020) at (a)–(e) daytime (9:30 a.m.), (e)–(h) nighttime (9:30 p.m.) and (k)–(o) day-night difference from ERA5 (unit: m s^{-1}). Shading shows wind speed, and vectors denote wind directions. Areas where day-night differences of wind speed do not pass the 95% confidence level (t-test) in (k–o) are masked out in grey. Only differences in wind vectors significant at the 95% confidence level are shown.

While surface winds can affect both the emissions and transport of dust from source regions, the dust uplift potential (DUP; Marsham et al., 2011) better quantifies the dust emission power of winds. Figure 12 shows the climatology of daytime, nighttime, and day-night differences in DUP calculated using surface wind speed from the ERA5 and a monthly 2D threshold velocity of wind erosion retrieved by Pu et al. (2020) using MODIS DOD, satellite retrieved land surface variables, and ERA5 surface winds. The seasonal climatology of DUP reveals that wind speed capable of dust emissions is predominantly in the northern part of the Sahel to the central Sahara, the Arabian Peninsula, and around the Taklamakan Desert, with the strongest DUP in MAM and JJA, and higher in the daytime (Fig. 12b–e) than nighttime (Fig. 12g–j). The day-night differences in DUP

https://doi.org/10.5194/acp-2022-490
Preprint. Discussion started: 4 October 2022

Atmospheric Chemistry and Physics Discussions

are positive and significant in the Sahara, the central to eastern Arabian Peninsula, and around the Taklamakan Desert, consistent with higher daytime DOD in these regions (Fig. 4l–o), indicating stronger daytime dust emissions and likely contribute to the positive day-night differences in DOD (Fig. 4). We also tried calculating DUP using a constant threshold wind velocity of 7 m s^{-1} following Marsham et al. (2011) and Bergametti et al. (2017), and the overall results are similar except the overall DUP is slightly lower and the day-night differences peak in MAM (Fig. S6).

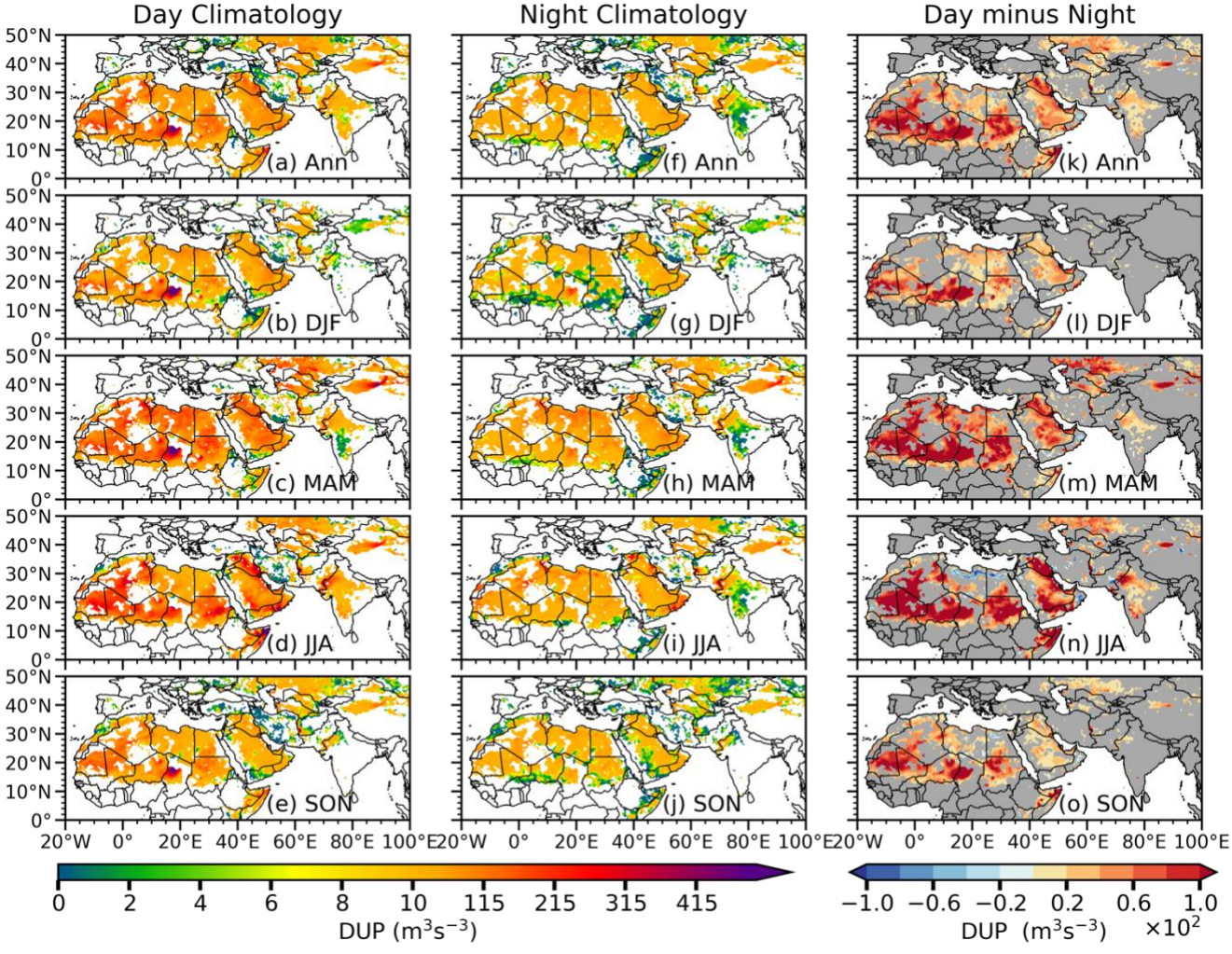

Figure 12: Annual (Ann) and seasonal mean climatology (2008–2020) of (a)–(e) dust uplift potential (DUP) at daytime (9:30 a.m.), (e)–(h) nighttime (9:30 p.m., e–h) and (k)–(o) day-night difference using wind velocity threshold estimated by Pu et al. (2020) and surface wind speed from the ERA5 (unit: m^3 s^{-3}). Areas where day-night differences of DUP do not pass the 95% confidence level (t-test) in (k–o) are masked out in grey.

What is the influence of surface winds on the diurnal cycle of dust activates at LISA and AERONET sites? Figure 13 shows the diurnal cycle of observed surface wind speed over LISA sites and ERA5 winds over AERONET sites. The cyan

https://doi.org/10.5194/acp-2022-490
Preprint. Discussion started: 4 October 2022


Atmospheric Chemistry and Physics Discussions

vertical lines mark the 9:30 a.m. and 9:30 p.m. LST. Surface wind speeds at LISA sites (Ban, Cin and Mbo) over the Sahel peak in the morning around 10–11 a.m. LST in most of the seasons except at Mbo site in JJA and SON, where surface winds maximize in the afternoon around 3–4 p.m. LST (Figs. 13a–c). A minimum of surface wind speed usually occurs in the evening around 8 p.m. or mid-night, with a secondary minimum around early morning (~ 7 a.m.). The diurnal cycle of surface PM_{10} concentrations show similar maxima in the late morning around 10–11 a.m. and minima in early morning around 6–7 a.m. (Fig. 8a–c), coinciding with the variations in surface wind speeds (Fig. 13a-c), which is consistent with the findings of Kaly et al. (2015). However, the evening maxima of PM_{10} concentrations around 6–8 p.m. (Fig. 8a–c) was not in correspondence with wind speed minima around the same time (Fig. 13a–c), suggesting that other factors in addition to surface winds may be contributing to the evening increase in PM_{10} concentrations.

The morning peaks (around 7–8 a.m. LST) of surface wind speed at AERONET stations in North Africa (Dak, Ilo, and Kof), in the Middle East (Mez), and the Indian subcontinent (Kan; Fig. 13 d–g, i) are consistent with the morning maxima of CAOD (Fig. 8d-g, i), while the wind speed minima in the late afternoon to evening (around 4–6 p.m.) and in early morning (5 a.m.) at most sites (Fig. 13 d–i) are also consistent with the minima of CAOD (Fig. 8 d–i). At Mez and Kof stations, the secondary peaks of CAOD in the afternoon or nighttime largely coincide with increases in surface wind speed but not so at sites such as Ilo and Kan. In short, the comparison between the diurnal cycle of surface wind speed and CAOD or PM_{10} concentrations reveal some similar diurnal variations, especially for the early morning minima of wind speed and CAOD or PM_{10} and the late morning maxima. Individual sites show some local features depending on their distances to dust sources and ocean, elevation, and seasonality.

https://doi.org/10.5194/acp-2022-490
Preprint. Discussion started: 4 October 2022

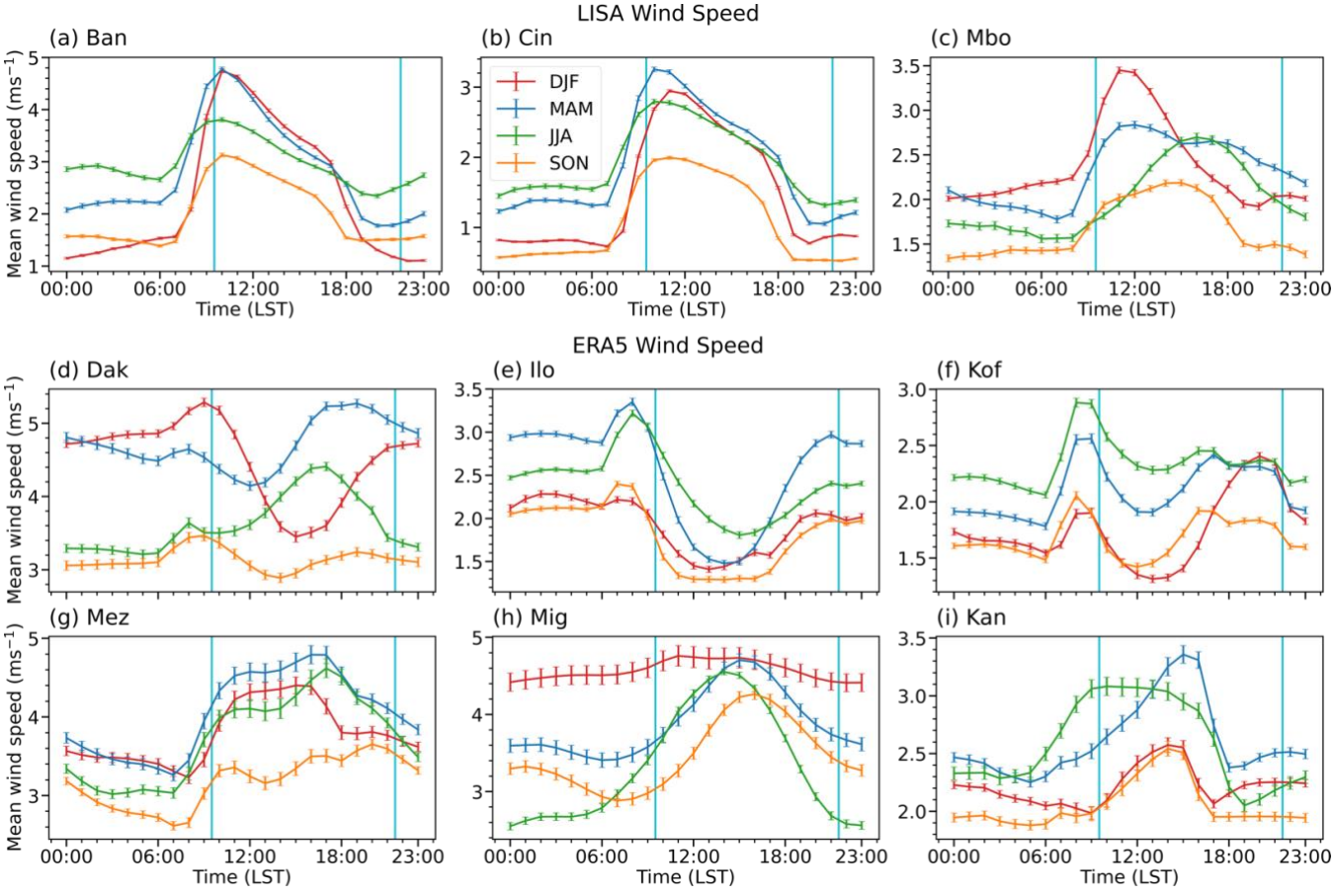

Figure 13: Diurnal cycle of (a)–(c) observed surface wind speed at LISA sites and (d)–(i) ERA5 surface wind speed over AERONET sites in different seasons averaged over 2008–2020 for Ban and Cin, 2008–2012 for Mbo of LISA sites, and over 2008–2020 for ERA5 (unit: m s^{-1}). The cyan vertical lines mark the ISAI passing time at 9:30 a.m. and 9:30 p.m. LST. Error bars show standard errors.

3.6.2 Precipitation

Precipitation is another factor that can influence the spatiotemporal variability of dust over the dust belt (Engelstaedter et al., 2006; Engelstaedter and Washington, 2007; Knippertz and Todd, 2012; Pu and Ginoux, 2018). Precipitation affects dust aerosols through wet deposition and increased soil moisture that modifies the threshold wind velocity for dust emissions. Shown in Fig. 14 is the annual and seasonal mean climatology of day-night differences in precipitation using hourly observations from IMERG at IASI observation times (9:30 a.m. and 9:30 p.m.). Precipitation is low over dust source regions, with higher values along the Guinea Coast in MAM and SON and extends to the southern Sahel in JJA. Over the Indian subcontinent, the precipitation maximum also occurs in JJA following the setup of summer monsoon. Nighttime precipitation rate is higher than daytime in most of the regions in the domain (Fig. 14k–o), with the largest differences in JJA. The slightly

https://doi.org/10.5194/acp-2022-490
Preprint. Discussion started: 4 October 2022

Atmospheric Chemistry and Physics Discussions

higher nighttime precipitation rate over some spots of the Sahara, the central Arabian Peninsula, and the northwestern Indian subcontinent (Fig. 14 m–o) may suppress dust emissions and partially contribute to higher daytime DOD in these regions (Fig. 4m–o). However, over the Guinea Coast and the central to southern Indian subcontinent, the higher precipitation rate at night is inconsistent with higher DOD, indicating that wet deposition may not be playing any significant role in controlling the observed negative day-night differences in IASI DOD. Because early precipitation events have the potential to affect dust aerosols at IASI passing times (9:30 a.m. and 9:30 p.m.), we also examined precipitation two hours prior to IASI observations as shown in Fig. S7. Those results show similar precipitation distribution over the dust belt but, slightly greater in magnitude, suggesting that precipitation may have peaked earlier than IASI sampling time.

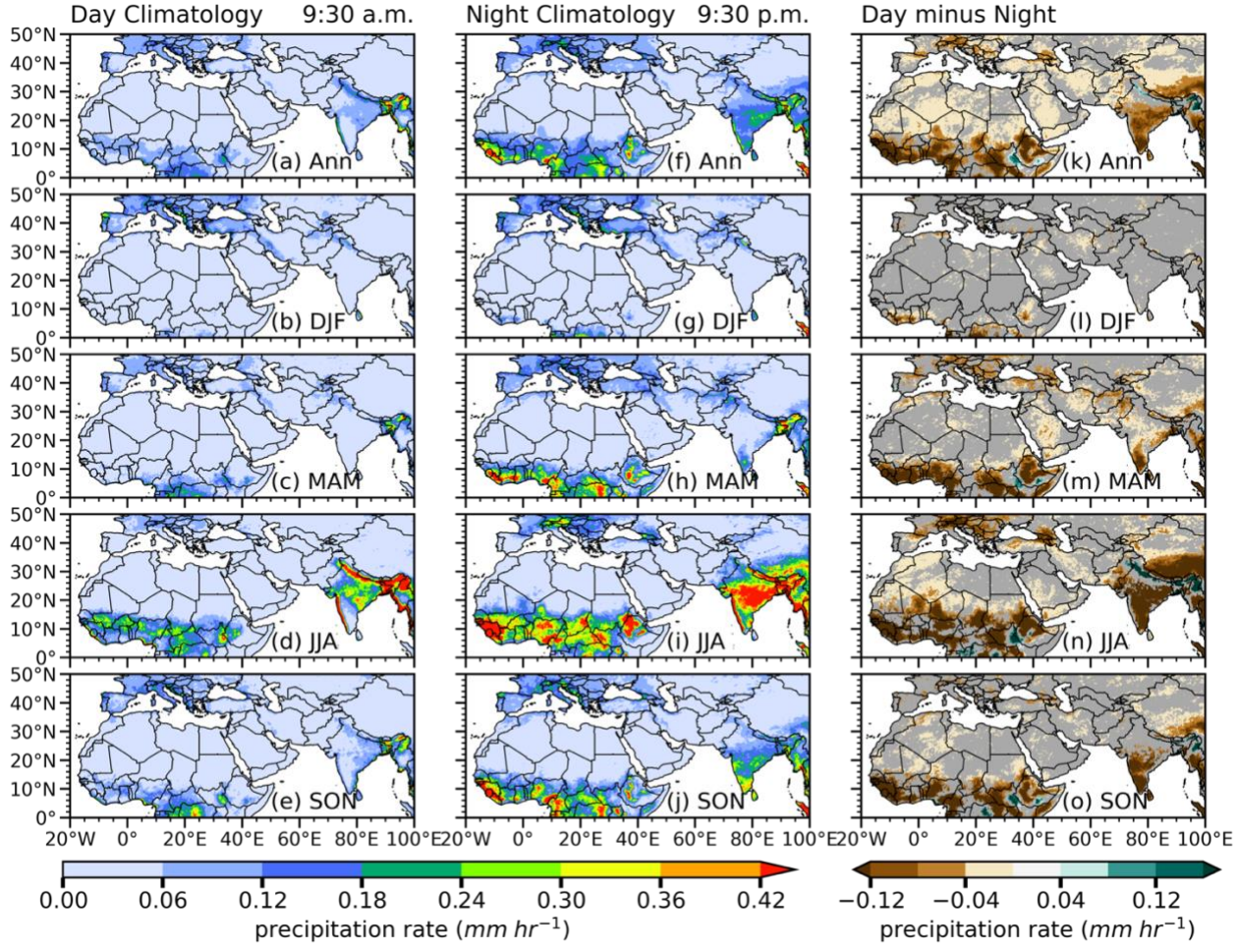

Figure 14: Annual (Ann) and seasonal mean climatology (2008–2020) of IMERG precipitation (mm hr^{-1}) at (a)–(e) daytime (9:30 a.m.), (f)–(j) nighttime (9:30 p.m.) and (k)–(o) day-night difference. Areas where day-night differences of precipitation do not pass the 95% confidence level (t-test) in (k–o) are masked out in grey.

https://doi.org/10.5194/acp-2022-490
Preprint. Discussion started: 4 October 2022

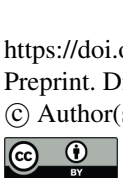

Atmospheric Chemistry and Physics Discussions

615

To further explore the impacts of the diurnal cycle of precipitation on dust activities we examined precipitation at LISA and AERONET stations using LISA and IMERG observations (Fig. 15). From LISA observations over the Sahel, precipitation peaks in JJA around early hours of the day (2 a.m. to 8 a.m.) over Ban and Cin (Fig. 15a, b) and late afternoon to early evening (2 p.m. to 7 p.m.) over Mbo (Fig. 15c) which is consistent with previous studies in this region (Marticorena et
620 al., 2010; Kaly et al., 2015). The higher precipitation rate from midnight to early morning in JJA can contribute to the lower daytime PM_{10} concentration in Ban and Cin (Fig. 8a, b and Fig. 15a, b). Mbo, on the other hand, has smaller day-night differences in PM_{10} concentrations and precipitation in JJA (Fig. 8c, 15c).

625

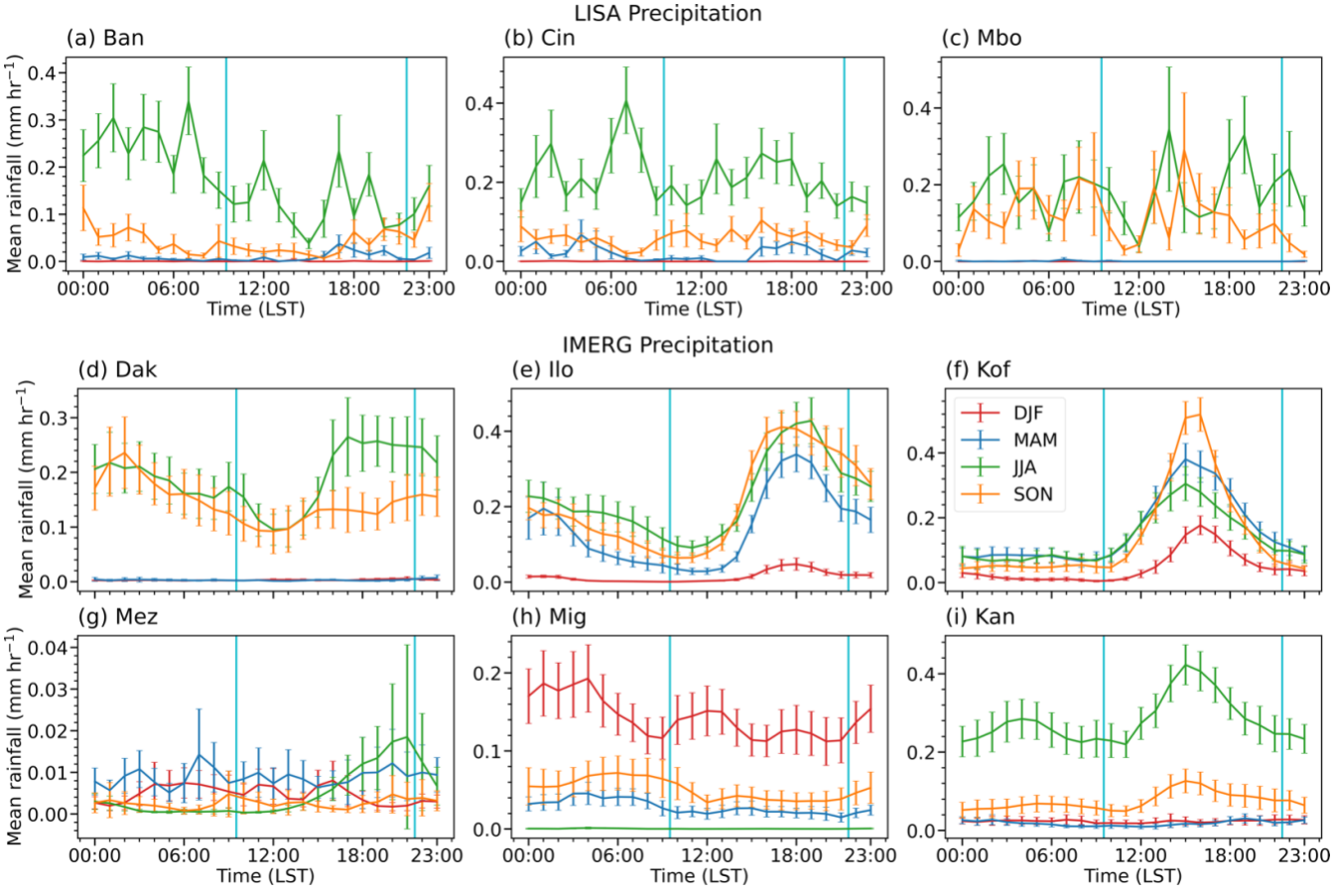

Figure 15: Diurnal cycle of (a)–(c) observed precipitation over LISA sites and (d)–(i) IMERG precipitation over AERONET sites in different seasons averaged over 2008–2020 for Ban and Cin, 2008–2012 for Mbo of LISA sites, and 2008-2020 for IMERG (unit: mm hr^{-1}). The cyan vertical lines mark IASI passing time at 9:30 a.m. and 9:30 p.m. LST. Error bars show the standard errors.

https://doi.org/10.5194/acp-2022-490
Preprint. Discussion started: 4 October 2022


Atmospheric Chemistry and Physics Discussions

Precipitation from IMERG reveals that Dak, which is collocated with LISA Mbo site, has a peak in JJA around 5 p.m. to 10 p.m. and in SON around 2 a.m. (Fig. 15d), which is somewhat different from station observations (Fig. 15c). The increase in precipitation in the afternoon and the maxima around 5–6 p.m. (3–4 p.m.) at Dak and Ilo (Kof) sites in JJA (Fig. 15d–f) roughly coincide with CAOD minima around 5–6 p.m. (Fig. 8d–f), suggesting that wet deposition reduces airborne dust. Nonetheless, at the Middle East and Asian sites, the precipitation maxima around 9 p.m. in JJA at Mez (Fig. 15g), 3 a.m. in DJF at Mig (Fig. 15h), and 3 p.m. in JJA at Kan (Fig. 15i) largely correspond to the peaks of CAOD, which suggests that wet scavenging is less important in driving the diurnal cycle of dust around these stations.

3.6.3 Boundary layer height and atmospheric stability

The planetary boundary layer (PBL) plays a vital role in regulating the vertical mixing and transport of near surface aerosols, including dust aerosols (Knippertz and Todd, 2012). A convective planetary boundary layer (PBL) on a clear, sunny day with low winds over desert regions can enhance dust emissions and vertical transport (Sinclair, 1969; Oke et al., 2007; Ansmann et al., 2009; Knippertz and Todd, 2012). For regions far away from dust sources with little local emissions, the rising boundary layer likely promote horizontal and vertical dispersal of aerosols, leading to reductions in their concentrations (Petäjä et al., 2016; Pal et al., 2014; Li et al., 2017; Lou et al., 2019). High concentrations of absorbing aerosols within the boundary layer can enhance the absorption and scattering of significant amount of solar radiation reaching the surface which reduces the sensible heat fluxes needed to drive the PBL evolution leading to a much shallow PBL height (PBLH; Li et al., 2017). A shallower PBLH can further increase surface concentration of aerosols leading to a positive feedback loop (Li et al., 2017). It is thus important to examine the impacts of the PBLH on the day-night differences in dust activities.

Figure 16 shows PBLH at daytime (9:30 a.m.), nighttime (9:30 p.m.), and the day-night differences over the dust belt from ERA5. The PBLH is highest during JJA at daytime, with higher values over the Guinea Coast, central Sahara, and large areas of Eurasia. In general, the day-night difference in PBLH is positive everywhere in the study domain, with smaller differences (0~400 m) over major dust source regions, e.g., the Sahara Deserts, the central to eastern Arabian Peninsula, and the Taklamakan Desert (except JJA) but larger differences (>400 m) over the Guinea coast, western Arabian Peninsula, large parts of the Indian subcontinent, and around the Taklamakan Desert (only in JJA; Fig. 16l–o). These results are consistent with similar analysis from MERRA-2 (Fig. S8) except MERRA-2 PBLH is much higher than that from ERA5, especially during the nighttime by about 1000~1500 m over the Sahara and the Arabian Peninsula. The discrepancies are largely due to different methods used to estimate PBLHs in the reanalyses, with the bulk Richardson number method being used in the ERA5 (Zhou et al., 2021).

A careful examination of these results reveals that the overall pattern of day-night differences in PBLH (Fig. 16k–o) is somewhat similar to the pattern of the day-night differences in dust layer height (Fig. 5k–o) but opposite to the structure of day-night difference in DOD (Fig. 4k–o) in IASI. The larger day-night differences in PBLH over the southern Sahel, the Guinea Coast, and the Indian subcontinent indicate that a growing PBL during daytime (9:30 a.m.) is likely entraining dust aerosols

https://doi.org/10.5194/acp-2022-490
Preprint. Discussion started: 4 October 2022

Atmospheric Chemistry and Physics Discussions

into higher altitudes where they are susceptible to upper-level horizontal transport. The dilution may contribute to the negative the day-night difference in DOD (i.e., lower daytime DOD than nighttime) in the regions.

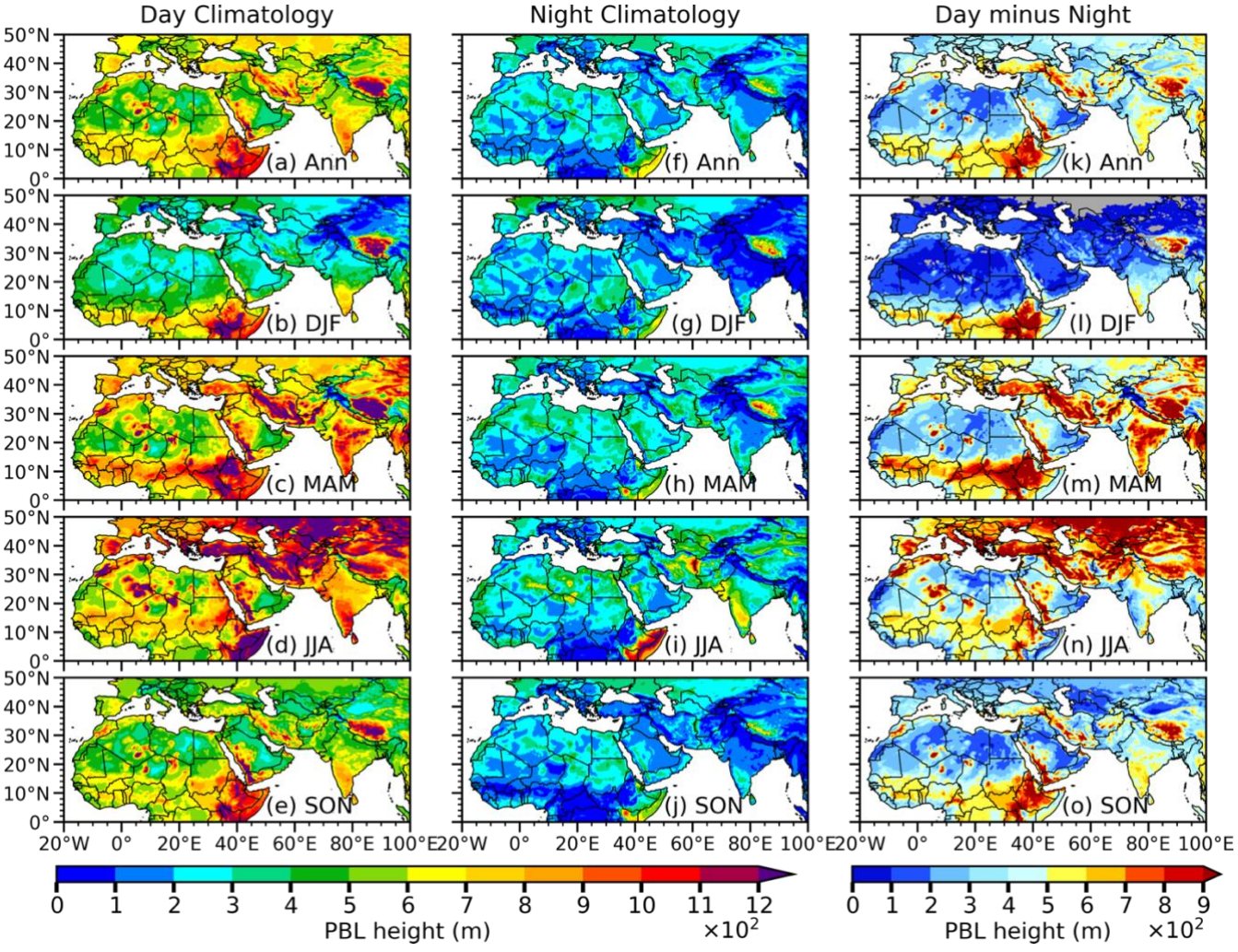

Figure 16: Annual (Ann) and seasonal mean climatology (2008–2020) of planetary boundary layer height (PBLH) at (a)–(e) daytime (9:30 a.m.), (f)–(j) nighttime (9:30 p.m.), and (k)–(o) day-night differences from the ERA5. Areas where day-night differences of PBLH do not pass the 95% confidence level (t-test) in (k–o) are masked out in grey.

An examination of the convective available potential energy (CAPE; Fig. 17) and vertical velocity at 850 hPa (Fig. S9) further show higher CAPE along with rising motion over the Sahel, the Guinea Coast, and the Indian subcontinent during the daytime (Figs. 17a-e, S9a-e), which may vertically mix dust aerosols into the free troposphere for horizontal dispersion, leading to lower dust concentrations and DOD and higher dust layer heights at daytime. For example, a higher daytime than nighttime CAPE over the southern Sahel (extending to the northern Sahel in JJA and SON; Fig. 17k–o), the Guinea Coast (DJF, MAM; Fig. 17l, m), and the central Indian subcontinent (MAM; Fig. 17m) is consistent with an upward motion in the southern parts of the Sahel, the Guinea Coast, and the central to the northern Indian subcontinent during the daytime (Fig. S9 b–e) and lower daytime DOD (Fig. 4k–o) and higher dust layer height (Fig. 5k–o).

https://doi.org/10.5194/acp-2022-490
Preprint. Discussion started: 4 October 2022

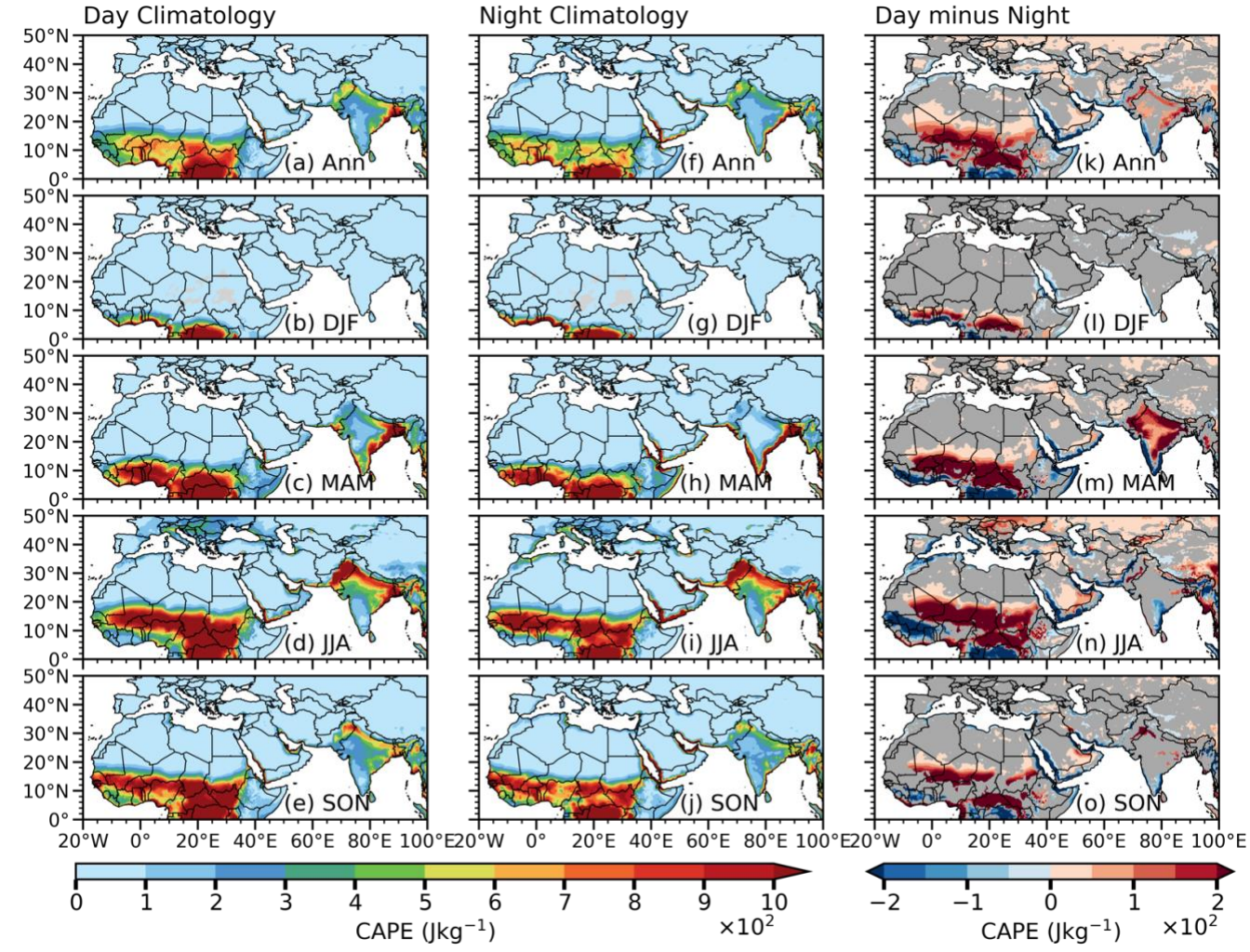

Figure 17: Annual (Ann) and Seasonal mean climatology (2008–2020) of convective available potential energy (CAPE) at (a)–(e) daytime (9:30 a.m.), (f)–(j) nighttime (9:30 p.m.), and (k)–(o) day-night differences from the ERA5. Areas where day-night differences of CAPE do not pass the 95% confidence level (t-test) in (k–o) are masked out in grey.

4 Discussion

While IASI products provide a viable source of information on global distribution of dust aerosols to complement ground observations, uncertainties associated with the limitations of the instrument, retrieval algorithm, and sampling frequency may add to the uncertainty of our findings. The inability of satellite to observe through clouds is a major setback in aerosol studies using satellite products (Schepanski et al., 2007; Heinold et al., 2013). IASI infrared sensor cannot observe dust aerosols under cloudy convective systems such as haboobs which often occur over North Africa in the evening periods, likely leading to a "morning bias" with more available data at 9:30 a.m. (Chédin et al., 2020). This could possibly affect the day-night

https://doi.org/10.5194/acp-2022-490
Preprint. Discussion started: 4 October 2022


Atmospheric Chemistry and Physics Discussions

differences in DOD and dust layer height observed from IASI over the convective regions (the Sahel, the Guinea Coast, and the Indian subcontinent) especially on the daily time scale, but likely has little effect on the monthly time scale or climatological mean (Chédin et al., 2020). On the other hand, a rigorous cloud masking method is used for LMD IASI products to ensure high confidence in cloud identification (Pierangelo et al., 2004; Crevoisier et al., 2009; Pernin et al., 2013; Capelle et al., 2018). Due to this, some aerosol loading, especially over the dust source regions, could be mistaken as clouds and screened out, leading to an underestimation of the actual DOD (Capelle et al., 2018).

Other possible sources of uncertainty of IASI retrievals include weak sensitivity to dust aerosols in the first hundred meters above the surface and difficulty in capturing low DOD of a similar order or smaller than the sensitivity of the instrument (Capelle et al. 2018). While the passing times of IASI largely coincide with the times of the two most important dust emission mechanisms in the Sahara Desert, i.e., breaking down of the nocturnal low-level jets in the morning and mesoscale convective systems (haboobs) at late afternoon to evening hours (Schepanski et al., 2009; Knippertz and Todd, 2012; Marsham et al., 2013; Chédin et al., 2020), some important dust events before and after the passage of IASI (9:30 a.m. and 9:30 p.m.) could be missed. Future studies of dust activities using instruments with different overpassing times likely will complement and improve our understanding of the diurnal cycle of dust aerosols. However, despite these challenges, the day-night differences in IASI DOD are largely consistent with the day-night differences in CAOD and PM_{10} concentrations from ground observations. The presence of orbital gabs around the tropics in current IASI products is partially addressed by the launches of IASI onboard MetOP-B and MetOP-C satellites in 2012 and 2018, respectively (Carboni et al., 2013; Klüser et al., 2013; Chédin et al., 2020). Future investigations using IASI from these satellites and algorithms different from LMD are warranted to confirm and overcome some of the limitations in this study.

In addition to the meteorological variables discussed above, we also found slightly higher relative humidity at 750 hPa at nighttime over the Guinea Coast and south coast of India (not shown) that may partially contribute to the higher nighttime DOD via the hygroscopic growth of aged dust, although the overall effect is hard to quantify in observations. Land surface variables such as soil moisture may also affect dust emissions in semi-arid regions. However, our examination of soil moisture from ERA5 showed insignificant day-night differences corresponding to the sampling time of IASI, indicating a likely negligible impact. While surface wind speed, precipitation, PBLH, and atmospheric stability all affect day-night differences in DOD and dust layer height to some extent, they may be fundamentally driven by common factors, such as diurnal cycle of surface radiation, and modulated by local land surface and circulation features. Additional sensitivity tests are needed to further quantify the relative contribution of individual factors to the day-night differences in dust activities revealed by IASI and station data and will be addressed in our future study.

5 Conclusions

While dust aerosol remains one of the key variables affecting the climate system, constraining the full diurnal cycle of dust from current visible satellite products and sparse in situ observations presents a challenge, which continues to contribute

https://doi.org/10.5194/acp-2022-490
Preprint. Discussion started: 4 October 2022


Atmospheric Chemistry and Physics Discussions

in large portion to the sources of uncertainties in estimating the total radiative forcing of aerosols and climate change projections. Using the equal quality performance for daytime (9:30 a.m.) and nighttime (9:30 p.m.) observations, and global coverage at fine spectral and spatial resolutions of IASI products, this study investigates the day-night differences in dust activities over the dust belt of North Africa, the Middle East, and Asia. A comparison between IASI 10 μm (converted to 500 nm) DOD and AERONET CAOD revealed an overall correlation coefficient of ~0.79 for 17 solar sites and ~0.6 for 10 lunar sites, indicating IASI exhibits high performance in capturing the spatiotemporal variability of dust events over the dust belt.

IASI showed significant (95% confidence level) day-night differences in DOD and dust layer height within the dust belt, with higher daytime DOD and lower dust layer height over dust source regions in the central to northern Sahara, the Arabian Peninsula, the northwestern Indian subcontinent, and the Taklamakan Desert. Over the southern Sahel to Guinea Coast and large area of the Indian Subcontinent, nighttime DOD is observed to be higher than daytime, along with lower dust layer height at nighttime. The day-night differences in DOD are larger and more significant in MAM and DJF than other seasons, while day-night differences in dust layer height show little seasonal variations. The higher daytime DOD in dust source regions (e.g., the central Sahara, the Arabian Peninsula, northwestern Indian subcontinent, and Taklamakan Desert) are likely associated with higher dust uplift potential (DUP) during daytime in these regions and larger magnitude of positive day-night differences in surface wind speeds in the Sahara Desert. Over some spots of the Sahara, the central Arabian Peninsula, and the northwestern Indian subcontinent, slightly higher nighttime precipitation rate may reduce airborne dust and partially contribute to higher daytime DOD from MAM to SON as well.

The low daytime DOD over downwind regions, such as the southern Sahel, Guinea Coast, and the central to southern Indian subcontinent, coincides with a relatively higher planetary boundary layer height (PBLH) and greater convective available potential energy (CAPE) at daytime that corresponds to an unstable atmosphere. The growing PBLH during the daytime likely entrains dust aerosols into upper levels, resulting in a higher dust layer height and favoring horizontal transport, which likely dilute column concentrations of dust and DOD during daytime.

Seasonal analysis of day-night differences in DOD from MERRA-2 and EAC4 revealed that reanalysis products largely capture the temporal and spatial variability of DOD on the seasonal scale but failed to capture the day-night differences in DOD in large parts of the dust belt except in a few dust hotspots over North Africa, such as the northeastern Bodélé Depression in DJF and MAM (MERRA-2), and over parts of northeastern North Africa in DJF, JJA and SON and over the southern Arabian Peninsula in DJF (MERRA-2 and EAC4).

Using in situ measurements from LISA and AERONET we have shown that dust aerosols exhibit a spatially varying diurnal cycle across the dust belt with higher coarse-mode aerosol optical depth (CAOD; around 7–9 a.m.) and PM_{10} concentrations (around 9–11 a.m.) in the morning hours and evening to midnight in the Sahel, higher CAOD from morning (7 or 9 a.m.) to noon and around late afternoon (3–4 p.m.) in the Arabian Peninsula and Indian subcontinent, with additional peaks around evening (Kan site). The day-night differences in CAOD between 9:30 a.m. and 9:30 p.m. are also largely consistent with day-night differences in IASI DOD in sign and magnitude, but not significant, possibly due to a smaller sample size of AERONET lunar data.

https://doi.org/10.5194/acp-2022-490
Preprint. Discussion started: 4 October 2022


Atmospheric Chemistry and Physics Discussions

In conclusion, this work has shown that daytime dust activities at 9:30 a.m. over the dust belt is significantly different from nighttime at 9:30 p.m., and such day-night differences are largely influenced by the local meteorological conditions, primarily, surface circulation, precipitation, and turbulent motion over the dust belt. Despite the uncertainties associated with satellite products, the findings add to our current understanding of the diurnal of cycle of dust in major dust source and downwind regions.

Data availability

Data used in this study can be downloaded from the links shown in Table 1.

Code availability

Analysis codes can be provided by the corresponding authors upon request.

Author contributions

BP and QJ conceived the study. JZT performed the analysis under the guidance of BP and QJ. JZT wrote the paper with input from BP and QJ.

Competing interest

The authors declare that they have no conflict of interest.

Acknowledgement

The authors would like to thank David Mechem and David Rahn for their helpful discussion and valuable suggestions on this paper. We also thank Brian Harr for helpful edits.

References

Ageet, S., Fink, A. H., Maranan, M., Diem, J. E., Hartter, J., Ssali, A. L., and Ayabagabo, P.: Validation of Satellite Rainfall Estimates over Equatorial East Africa, J. Hydrometeorol., 23, 129–151, https://doi.org/10.1175/JHM-D-21-0145.1, 2022.

Ansmann, A., Tesche, M., Knippertz, P., Bierwirth, E., Althausen, D., MüLLER, D., and Schulz, O.: Vertical profiling of convective dust plumes in southern Morocco during SAMUM, Tellus B Chem. Phys. Meteorol., 61, 340–353, https://doi.org/10.1111/j.1600-0889.2008.00384.x, 2009.

Arshad, M., Ma, X., Yin, J., Ullah, W., Ali, G., Ullah, S., Liu, M., Shahzaman, M., and Ullah, I.: Evaluation of GPM-IMERG and TRMM-3B42 precipitation products over Pakistan, Atmospheric Res., 249, 105341, https://doi.org/10.1016/j.atmosres.2020.105341, 2021.

https://doi.org/10.5194/acp-2022-490
Preprint. Discussion started: 4 October 2022

Bangert, M., Nenes, A., Vogel, B., Vogel, H., Barahona, D., Karydis, V. A., Kumar, P., Kottmeier, C., and Blahak, U.: Saharan dust event impacts on cloud formation and radiation over Western Europe, Atmospheric Chem. Phys., 12, 4045–4063, https://doi.org/10.5194/acp-12-4045-2012, 2012.

Bergametti, G., Marticorena, B., Rajot, J. L., Chatenet, B., Féron, A., Gaimoz, C., Siour, G., Coulibaly, M., Koné, I., Maman, A., and Zakou, A.: Dust Uplift Potential in the Central Sahel: An Analysis Based on 10 years of Meteorological Measurements at High Temporal Resolution, J. Geophys. Res. Atmospheres, 122, 12,433-12,448, https://doi.org/10.1002/2017JD027471, 2017a.

Bergametti, G., Marticorena, B., Rajot, J. L., Chatenet, B., Féron, A., Gaimoz, C., Siour, G., Coulibaly, M., Koné, I., Maman, A., and Zakou, A.: Dust Uplift Potential in the Central Sahel: An Analysis Based on 10 years of Meteorological Measurements at High Temporal Resolution, J. Geophys. Res. Atmospheres, 122, 12,433-12,448, https://doi.org/10.1002/2017JD027471, 2017b.

Berkoff, T. A., Sorokin, M., Stone, T., Eck, T. F., Hoff, R., Welton, E., and Holben, B.: Nocturnal Aerosol Optical Depth Measurements with a Small-Aperture Automated Photometer Using the Moon as a Light Source, J. Atmospheric Ocean. Technol., 28, 1297–1306, https://doi.org/10.1175/JTECH-D-10-05036.1, 2011.

Blumstein, D., Chalon, G., Carlier, T., Buil, C., Hebert, P., Maciaszek, T., Ponce, G., Phulpin, T., Tournier, B., Simeoni, D., Astruc, P., Clauss, A., Kayal, G., and Jegou, R.: IASI instrument: technical overview and measured performances, in: Infrared Spaceborne Remote Sensing XII, Infrared Spaceborne Remote Sensing XII, 196–207, https://doi.org/10.1117/12.560907, 2004.

Bozzo, A., Rémy, S., Benedetti, A., Flemming, J., Bechtold, P., Rodwell, M., and Morcrette, J.-J.: Implementation of a CAMS-based aerosol climatology in the IFS, 2017.

Bristow, C. S., Hudson-Edwards, K. A., and Chappell, A.: Fertilizing the Amazon and equatorial Atlantic with West African dust, Geophys. Res. Lett., 37, https://doi.org/10.1029/2010GL043486, 2010.

Capelle, V., Chédin, A., Siméon, M., Tsamalis, C., Pierangelo, C., Pondrom, M., Crevoisier, C., Crepeau, L., and Scott, N. A.: Evaluation of IASI-derived dust aerosol characteristics over the tropical belt, Atmospheric Chem. Phys., 14, 9343–9362, https://doi.org/10.5194/acp-14-9343-2014, 2014a.

Capelle, V., Chédin, A., Siméon, M., Tsamalis, C., Pierangelo, C., Pondrom, M., Crevoisier, C., Crepeau, L., and Scott, N. A.: over the tropical belt, 2014b.

Capelle, V., Chédin, A., Pondrom, M., Crevoisier, C., Armante, R., Crepeau, L., and Scott, N. A.: Infrared dust aerosol optical depth retrieved daily from IASI and comparison with AERONET over the period 2007–2016, Remote Sens. Environ., 206, 15–32, https://doi.org/10.1016/j.rse.2017.12.008, 2018.

Carboni, E., Smith, A., Grainger, R., Dudhia, A., Thomas, G., Peters, D., Walker, J., and Siddans, R.: Satellite remote sensing of volcanic plume from Infrared Atmospheric Sounding Interferometer (IASI): results for recent eruptions., in: EGU General Assembly Conference Abstracts, EGU2013-11865, 2013.

Carmona, J. M., Gupta, P., Lozano-García, D. F., Vanoye, A. Y., Yépez, F. D., and Mendoza, A.: Spatial and Temporal Distribution of PM2.5 Pollution over Northeastern Mexico: Application of MERRA-2 Reanalysis Datasets, Remote Sens., 12, 2286, https://doi.org/10.3390/rs12142286, 2020.

Chaboureau, J.-P., Tulet, P., and Mari, C.: Diurnal cycle of dust and cirrus over West Africa as seen from Meteosat Second Generation satellite and a regional forecast model, Geophys. Res. Lett., 34, https://doi.org/10.1029/2006GL027771, 2007.

Checa-Garcia, R., Balkanski, Y., Albani, S., Bergman, T., Carslaw, K., Cozic, A., Dearden, C., Marticorena, B., Michou, M., van Noije, T., Nabat, P., O'Connor, F. M., Olivié, D., Prospero, J. M., Le Sager, P., Schulz, M., and Scott, C.: Evaluation of natural aerosols in CRESCENDO Earth system models (ESMs): mineral dust, Atmospheric Chem. Phys., 21, 10295–10335, https://doi.org/10.5194/acp-21-10295-2021, 2021.

Chédin, A., Capelle, V., Scott, N. A., and Todd, M. C.: Contribution of IASI to the Observation of Dust Aerosol Emissions (Morning and Nighttime) Over the Sahara Desert, J. Geophys. Res. Atmospheres, 125, e32014, https://doi.org/10.1029/2019JD032014, 2020a.

Chédin, A., Capelle, V., Scott, N. A., and Todd, M. C.: Contribution of IASI to the Observation of Dust Aerosol Emissions (Morning and Nighttime) Over the Sahara Desert, J. Geophys. Res. Atmospheres, 125, e2019JD032014, https://doi.org/10.1029/2019JD032014, 2020b.

Clarisse, L., Clerbaux, C., Franco, B., Hadji-Lazaro, J., Whitburn, S., Kopp, A. K., Hurtmans, D., and Coheur, P.-F.: A Decadal Data Set of Global Atmospheric Dust Retrieved From IASI Satellite Measurements, J. Geophys. Res. Atmospheres, 124, 1618–1647, https://doi.org/10.1029/2018JD029701, 2019.

Crevoisier, C., Nobileau, D., Fiore, A. M., Armante, R., Chédin, A., and Scott, N. A.: Tropospheric methane in the tropics – first year from IASI hyperspectral infrared observations, Atmospheric Chem. Phys., 9, 6337–6350, https://doi.org/10.5194/acp-9-6337-2009, 2009.

D'Almeida, G. A.: A Model for Saharan Dust Transport, J. Appl. Meteorol. Climatol., 25, 903–916, https://doi.org/10.1175/1520-0450(1986)025<0903:AMFSDT>2.0.CO;2, 1986.

DeMott, P. J., Sassen, K., Poellot, M. R., Baumgardner, D., Rogers, D. C., Brooks, S. D., Prenni, A. J., and Kreidenweis, S. M.: African dust aerosols as atmospheric ice nuclei, Geophys. Res. Lett., 30, https://doi.org/10.1029/2003GL017410, 2003.

Dezfuli, A. K., Ichoku, C. M., Huffman, G. J., Mohr, K. I., Selker, J. S., Giesen, N. van de, Hochreutener, R., and Annor, F. O.: Validation of IMERG Precipitation in Africa, J. Hydrometeorol., 18, 2817–2825, https://doi.org/10.1175/JHM-D-17-0139.1, 2017.

Diner, D. J., Beckert, J. C., Reilly, T. H., Bruegge, C. J., Conel, J. E., Kahn, R. A., Martonchik, J. V., Ackerman, T. P., Davies, R., Gerstl, S. A. W., Gordon, H. R., Muller, J.-P., Myneni, R. B., Sellers, P. J., Pinty, B., and Verstraete, M. M.: Multi-angle Imaging SpectroRadiometer (MISR) instrument description and experiment overview, IEEE Trans. Geosci. Remote Sens., 36, 1072–1087, https://doi.org/10.1109/36.700992, 1998.

Duce, R. A.: Sources, distributions, and fluxes of mineral aerosols and their relationship to climate, Aerosol Forcing Clim., 6, 43–72, 1995.

Duce, R. A. and Tindale, N. W.: Atmospheric transport of iron and its deposition in the ocean, Limnol. Oceanogr., 36, 1715–1726, https://doi.org/10.4319/lo.1991.36.8.1715, 1991.

Dunion, J. P. and Velden, C. S.: The Impact of the Saharan Air Layer on Atlantic Tropical Cyclone Activity, Bull. Am. Meteorol. Soc., 85, 353–366, https://doi.org/10.1175/BAMS-85-3-353, 2004.

Eck, T. F., Holben, B. N., Reid, J. S., Dubovik, O., Smirnov, A., O'Neill, N. T., Slutsker, I., and Kinne, S.: Wavelength dependence of the optical depth of biomass burning, urban, and desert dust aerosols, J. Geophys. Res. Atmospheres, 104, 31333–31349, https://doi.org/10.1029/1999JD900923, 1999.

Eck, T. F., Holben, B. N., Sinyuk, A., Pinker, R. T., Goloub, P., Chen, H., Chatenet, B., Li, Z., Singh, R. P., Tripathi, S. N., Reid, J. S., Giles, D. M., Dubovik, O., O'Neill, N. T., Smirnov, A., Wang, P., and Xia, X.: Climatological aspects of the optical properties of fine/coarse mode aerosol mixtures, J. Geophys. Res., 115, D19205, https://doi.org/10.1029/2010JD014002, 2010.

Engelstaedter, S. and Washington, R.: Temporal controls on global dust emissions: The role of surface gustiness, Geophys. Res. Lett., 34, https://doi.org/10.1029/2007GL029971, 2007.

Engelstaedter, S., Tegen, I., and Washington, R.: North African dust emissions and transport, Earth-Sci. Rev., 79, 73–100, https://doi.org/10.1016/j.earscirev.2006.06.004, 2006.

Fernandez-Partagas, J., Helgren, D. M., and Prospero, J. M.: Threshold Wind Volocities for Raising Dust in the Western Sahara., ROSENSTIEL SCHOOL OF MARINE AND ATMOSPHERIC SCIENCE MIAMI FL, 1986.

Fiedler, S., Schepanski, K., Heinold, B., Knippertz, P., and Tegen, I.: Climatology of nocturnal low-level jets over North Africa and implications for modeling mineral dust emission, J. Geophys. Res. Atmospheres, 118, 6100–6121, https://doi.org/10.1002/jgrd.50394, 2013.

Flamant, C., Chaboureau, J.-P., Parker, D. J., Taylor, C. M., Cammas, J.-P., Bock, O., Timouk, F., and Pelon, J.: Airborne observations of the impact of a convective system on the planetary boundary layer thermodynamics and aerosol distribution in the inter-tropical discontinuity region of the West African Monsoon, Q. J. R. Meteorol. Soc., 133, 1175–1189, https://doi.org/10.1002/qj.97, 2007.

Forster, P., Ramaswamy, V., Artaxo, P., Berntsen, T., Betts, R., Fahey, D. W., Haywood, J., Lean, J., Lowe, D. C., Myhre, G., Nganga, J., Prinn, R., Raga, G., Schulz, M., and Van Dorland, R.: Changes in Atmospheric Constituents and in Radiative Forcing. Chapter 2, Clim. Change 2007 Phys. Sci. Basis, 2007.

Gelaro, R., McCarty, W., Suárez, M. J., Todling, R., Molod, A., Takacs, L., Randles, C. A., Darmenov, A., Bosilovich, M. G., Reichle, R., Wargan, K., Coy, L., Cullather, R., Draper, C., Akella, S., Buchard, V., Conaty, A., Silva, A. M. da, Gu, W., Kim, G.-K., Koster, R., Lucchesi, R., Merkova, D., Nielsen, J. E., Partyka, G., Pawson, S., Putman, W., Rienecker, M., Schubert, S. D., Sienkiewicz, M., and Zhao, B.: The Modern-Era Retrospective Analysis for Research and Applications, Version 2 (MERRA-2), J. Clim., 30, 5419–5454, https://doi.org/10.1175/JCLI-D-16-0758.1, 2017.

Ginoux, P., Chin, M., Tegen, I., Prospero, J. M., Holben, B., Dubovik, O., and Lin, S.-J.: Sources and distributions of dust aerosols simulated with the GOCART model, J. Geophys. Res. Atmospheres, 106, 20255–20273, https://doi.org/10.1029/2000JD000053, 2001.

Ginoux, P., Prospero, J. M., Gill, T. E., Hsu, N. C., and Zhao, M.: Global-scale attribution of anthropogenic and natural dust sources and their emission rates based on MODIS Deep Blue aerosol products, Rev. Geophys., 50, https://doi.org/10.1029/2012RG000388, 2012.

Goudie, A. S. and Middleton, N. J.: Desert Dust in the Global System, Springer Science & Business Media, 287 pp., 2006.

Grandey, B. S., Stier, P., and Wagner, T. M.: Investigating relationships between aerosol optical depth and cloud fraction using satellite, aerosol reanalysis and general circulation model data, Atmospheric Chem. Phys., 13, 3177–3184, https://doi.org/10.5194/acp-13-3177-2013, 2013.

Haywood, J. M., Allan, R. P., Culverwell, I., Slingo, T., Milton, S., Edwards, J., and Clerbaux, N.: Can desert dust explain the outgoing longwave radiation anomaly over the Sahara during July 2003?, J. Geophys. Res. Atmospheres, 110, https://doi.org/10.1029/2004JD005232, 2005.

https://doi.org/10.5194/acp-2022-490
Preprint. Discussion started: 4 October 2022


Atmospheric Chemistry and Physics Discussions

Heinold, B., Knippertz, P., Marsham, J. H., Fiedler, S., Dixon, N. S., Schepanski, K., Laurent, B., and Tegen, I.: The role of deep convection and nocturnal low-level jets for dust emission in summertime West Africa: Estimates from convection-permitting simulations, J. Geophys. Res. Atmospheres, 118, 4385–4400, https://doi.org/10.1002/jgrd.50402, 2013.

Hersbach, H., Bell, B., Berrisford, P., Hirahara, S., Horányi, A., Muñoz-Sabater, J., Nicolas, J., Peubey, C., Radu, R., Schepers, D., Simmons, A., Soci, C., Abdalla, S., Abellan, X., Balsamo, G., Bechtold, P., Biavati, G., Bidlot, J., Bonavita, M., Chiara, G., Dahlgren, P., Dee, D., Diamantakis, M., Dragani, R., Flemming, J., Forbes, R., Fuentes, M., Geer, A., Haimberger, L., Healy, S., Hogan, R. J., Hólm, E., Janisková, M., Keeley, S., Laloyaux, P., Lopez, P., Lupu, C., Radnoti, G., Rosnay, P., Rozum, I., Vamborg, F., Villaume, S., and Thépaut, J.: The ERA5 global reanalysis, Q. J. R. Meteorol. Soc., qj.3803, https://doi.org/10.1002/qj.3803, 2020.

Hewison, T. J., Wu, X., Yu, F., Tahara, Y., Hu, X., Kim, D., and Koenig, M.: GSICS Inter-Calibration of Infrared Channels of Geostationary Imagers Using Metop/IASI, IEEE Trans. Geosci. Remote Sens., 51, 1160–1170, https://doi.org/10.1109/TGRS.2013.2238544, 2013.

Holben, B. N., Eck, T. F., Slutsker, I., Tanré, D., Buis, J. P., Setzer, A., Vermote, E., Reagan, J. A., Kaufman, Y. J., Nakajima, T., Lavenu, F., Jankowiak, I., and Smirnov, A.: AERONET—A Federated Instrument Network and Data Archive for Aerosol Characterization, Remote Sens. Environ., 66, 1–16, https://doi.org/10.1016/S0034-4257(98)00031-5, 1998.

Hosseini-Moghari, S.-M. and Tang, Q.: Validation of GPM IMERG V05 and V06 Precipitation Products over Iran, J. Hydrometeorol., 21, 1011–1037, https://doi.org/10.1175/JHM-D-19-0269.1, 2020.

Huang, W.-R., Chang, Y.-H., and Liu, P.-Y.: Assessment of IMERG precipitation over Taiwan at multiple timescales, Atmospheric Res., 214, 239–249, https://doi.org/10.1016/j.atmosres.2018.08.004, 2018.

Huffman, G. J., Bolvin, D. T., Braithwaite, D., Hsu, K., Joyce, R., Xie, P., and Yoo, S.-H.: NASA global precipitation measurement (GPM) integrated multi-satellite retrievals for GPM (IMERG), Algorithm Theor. Basis Doc. ATBD Version, 4, 26, 2015.

Huneeus, N., Schulz, M., Balkanski, Y., Griesfeller, J., Prospero, J., Kinne, S., Bauer, S., Boucher, O., Chin, M., Dentener, F., Diehl, T., Easter, R., Fillmore, D., Ghan, S., Ginoux, P., Grini, A., Horowitz, L., Koch, D., Krol, M. C., Landing, W., Liu, X., Mahowald, N., Miller, R., Morcrette, J.-J., Myhre, G., Penner, J., Perlwitz, J., Stier, P., Takemura, T., and Zender, C. S.: Global dust model intercomparison in AeroCom phase I, Atmospheric Chem. Phys., 11, 7781–7816, https://doi.org/10.5194/acp-11-7781-2011, 2011.

Inness, A., Ades, M., Agustí-Panareda, A., Barré, J., Benedictow, A., Blechschmidt, A.-M., Dominguez, J. J., Engelen, R., Eskes, H., Flemming, J., Huijnen, V., Jones, L., Kipling, Z., Massart, S., Parrington, M., Peuch, V.-H., Razinger, M., Remy, S., Schulz, M., and Suttie, M.: The CAMS reanalysis of atmospheric composition, Atmospheric Chem. Phys., 19, 3515–3556, https://doi.org/10.5194/acp-19-3515-2019, 2019.

Isaza, A., Kay, M., Evans, J. P., Bremner, S., and Prasad, A.: Validation of Australian atmospheric aerosols from reanalysis data and CMIP6 simulations, Atmospheric Res., 264, 105856, https://doi.org/10.1016/j.atmosres.2021.105856, 2021.

Jickells, T. D., An, Z. S., Andersen, K. K., Baker, A. R., Bergametti, G., Brooks, N., Cao, J. J., Boyd, P. W., Duce, R. A., Hunter, K. A., Kawahata, H., Kubilay, N., laRoche, J., Liss, P. S., Mahowald, N., Prospero, J. M., Ridgwell, A. J., Tegen, I., and Torres, R.: Global Iron Connections Between Desert Dust, Ocean Biogeochemistry, and Climate, Science, 308, 67–71, https://doi.org/10.1126/science.1105959, 2005.

Jin, Q., Wei, J., and Yang, Z.-L.: Positive response of Indian summer rainfall to Middle East dust, Geophys. Res. Lett., 41, 4068–4074, https://doi.org/10.1002/2014GL059980, 2014.

945 Jin, Q., Wei, J., Yang, Z.-L., Pu, B., and Huang, J.: Consistent response of Indian summer monsoon to Middle East dust in observations and simulations, Atmospheric Chem. Phys., 15, 9897–9915, https://doi.org/10.5194/acp-15-9897-2015, 2015.

Jin, Q., Yang, Z.-L., and Wei, J.: Seasonal Responses of Indian Summer Monsoon to Dust Aerosols in the Middle East, India, and China, J. Clim., 29, 6329–6349, https://doi.org/10.1175/JCLI-D-15-0622.1, 2016.

Jin, Q., Wei, J., Lau, W. K. M., Pu, B., and Wang, C.: Interactions of Asian mineral dust with Indian summer monsoon: Recent
950 advances and challenges, Earth-Sci. Rev., 215, 103562, https://doi.org/10.1016/j.earscirev.2021.103562, 2021.

Kaly, F., Marticorena, B., Chatenet, B., Rajot, J. L., Janicot, S., Niang, A., Yahi, H., Thiria, S., Maman, A., Zakou, A., Coulibaly, B. S., Coulibaly, M., Koné, I., Traoré, S., Diallo, A., and Ndiaye, T.: Variability of mineral dust concentrations over West Africa monitored by the Sahelian Dust Transect, Atmospheric Res., 164–165, 226–241, https://doi.org/10.1016/j.atmosres.2015.05.011, 2015.

955 Karyampudi, V. M. and Carlson, T. N.: Analysis and Numerical Simulations of the Saharan Air Layer and Its Effect on Easterly Wave Disturbances, J. Atmospheric Sci., 45, 3102–3136, https://doi.org/10.1175/1520-0469(1988)045<3102:AANSOT>2.0.CO;2, 1988.

Kim, K., Park, J., Baik, J., and Choi, M.: Evaluation of topographical and seasonal feature using GPM IMERG and TRMM 3B42 over Far-East Asia, Atmospheric Res., 187, 95–105, https://doi.org/10.1016/j.atmosres.2016.12.007, 2017.

960 Klüser, L., Erbertseder, T., and Meyer-Arnek, J.: Observation of volcanic ash from Puyehue–Cordón Caulle with IASI, Atmospheric Meas. Tech., 6, 35–46, https://doi.org/10.5194/amt-6-35-2013, 2013.

Knippertz, P.: Meteorological Aspects of Dust Storms, in: Mineral Dust: A Key Player in the Earth System, edited by: Knippertz, P. and Stuut, J.-B. W., Springer Netherlands, Dordrecht, 121–147, https://doi.org/10.1007/978-94-017-8978-3_6, 2014.

965 Knippertz, P. and Todd, M. C.: Mineral dust aerosols over the Sahara: Meteorological controls on emission and transport and implications for modeling, Rev. Geophys., 50, https://doi.org/10.1029/2011RG000362, 2012.

Kocha, C., Tulet, P., Lafore, J.-P., and Flamant, C.: The importance of the diurnal cycle of Aerosol Optical Depth in West Africa, Geophys. Res. Lett., 40, 785–790, https://doi.org/10.1002/grl.50143, 2013.

Kok, J. F., Adebiyi, A. A., Albani, S., Balkanski, Y., Checa-Garcia, R., Chin, M., Colarco, P. R., Hamilton, D. S., Huang, Y.,
970 Ito, A., Klose, M., Li, L., Mahowald, N. M., Miller, R. L., Obiso, V., Pérez García-Pando, C., Rocha-Lima, A., and Wan, J. S.: Contribution of the world's main dust source regions to the global cycle of desert dust, Atmospheric Chem. Phys., 21, 8169–8193, https://doi.org/10.5194/acp-21-8169-2021, 2021.

Kylling, A., Vandenbussche, S., Capelle, V., Cuesta, J., Klüser, L., Lelli, L., Popp, T., Stebel, K., and Veefkind, P.: Comparison of dust-layer heights from active and passive satellite sensors, Atmospheric Meas. Tech., 11, 2911–2936,
975 https://doi.org/10.5194/amt-11-2911-2018, 2018.

Lee, J., Lee, E.-H., and Seol, K.-H.: Validation of Integrated MultisatellitE Retrievals for GPM (IMERG) by using gauge-based analysis products of daily precipitation over East Asia, Theor. Appl. Climatol., 137, 2497–2512, https://doi.org/10.1007/s00704-018-2749-1, 2019.

Levin, Z., Ganor, E., and Gladstein, V.: The Effects of Desert Particles Coated with Sulfate on Rain Formation in the Eastern
980 Mediterranean, J. Appl. Meteorol. Climatol., 35, 1511–1523, https://doi.org/10.1175/1520-0450(1996)035<1511:TEODPC>2.0.CO;2, 1996.

https://doi.org/10.5194/acp-2022-490
Preprint. Discussion started: 4 October 2022

Li, F., Vogelmann, A. M., and Ramanathan, V.: Saharan Dust Aerosol Radiative Forcing Measured from Space, J. Clim., 17, 2558–2571, https://doi.org/10.1175/1520-0442(2004)017<2558:SDARFM>2.0.CO;2, 2004.

Li, J., Ge, X., He, Q., and Abbas, A.: Aerosol optical depth (AOD): spatial and temporal variations and association with meteorological covariates in Taklimakan desert, China, PeerJ, 9, e10542, https://doi.org/10.7717/peerj.10542, 2021.

Li, Z., Guo, J., Ding, A., Liao, H., Liu, J., Sun, Y., Wang, T., Xue, H., Zhang, H., and Zhu, B.: Aerosol and boundary-layer interactions and impact on air quality, Natl. Sci. Rev., 4, 810–833, https://doi.org/10.1093/nsr/nwx117, 2017.

Liu, Z., Vaughan, M., Winker, D., Kittaka, C., Getzewich, B., Kuehn, R., Omar, A., Powell, K., Trepte, C., and Hostetler, C.: The CALIPSO Lidar Cloud and Aerosol Discrimination: Version 2 Algorithm and Initial Assessment of Performance, J. Atmospheric Ocean. Technol., 26, 1198–1213, https://doi.org/10.1175/2009JTECHA1229.1, 2009.

Lou, M., Guo, J., Wang, L., Xu, H., Chen, D., Miao, Y., Lv, Y., Li, Y., Guo, X., Ma, S., and Li, J.: On the Relationship Between Aerosol and Boundary Layer Height in Summer in China Under Different Thermodynamic Conditions, Earth Space Sci., 6, 887–901, https://doi.org/10.1029/2019EA000620, 2019.

Mahowald, N. M., Kloster, S., Engelstaedter, S., Moore, J. K., Mukhopadhyay, S., McConnell, J. R., Albani, S., Doney, S. C., Bhattacharya, A., Curran, M. A. J., Flanner, M. G., Hoffman, F. M., Lawrence, D. M., Lindsay, K., Mayewski, P. A., Neff, J., Rothenberg, D., Thomas, E., Thornton, P. E., and Zender, C. S.: Observed 20th century desert dust variability: impact on climate and biogeochemistry, Atmospheric Chem. Phys., 10, 10875–10893, https://doi.org/10.5194/acp-10-10875-2010, 2010.

Maranan, M., Fink, A. H., Knippertz, P., Amekudzi, L. K., Atiah, W. A., and Stengel, M.: A Process-Based Validation of GPM IMERG and Its Sources Using a Mesoscale Rain Gauge Network in the West African Forest Zone, J. Hydrometeorol., 21, 729–749, https://doi.org/10.1175/JHM-D-19-0257.1, 2020.

Marsham, J. H., Parker, D. J., Grams, C. M., Taylor, C. M., and Haywood, J. M.: Uplift of Saharan dust south of the intertropical discontinuity, J. Geophys. Res. Atmospheres, 113, https://doi.org/10.1029/2008JD009844, 2008.

Marsham, J. H., Knippertz, P., Dixon, N. S., Parker, D. J., and Lister, G. M. S.: The importance of the representation of deep convection for modeled dust-generating winds over West Africa during summer, Geophys. Res. Lett., 38, https://doi.org/10.1029/2011GL048368, 2011.

Marsham, J. H., Hobby, M., Allen, C. J. T., Banks, J. R., Bart, M., Brooks, B. J., Cavazos-Guerra, C., Engelstaedter, S., Gascoyne, M., Lima, A. R., Martins, J. V., McQuaid, J. B., O'Leary, A., Ouchene, B., Ouladichir, A., Parker, D. J., Saci, A., Salah-Ferroudj, M., Todd, M. C., and Washington, R.: Meteorology and dust in the central Sahara: Observations from Fennec supersite-1 during the June 2011 Intensive Observation Period, J. Geophys. Res. Atmospheres, 118, 4069–4089, https://doi.org/10.1002/jgrd.50211, 2013.

Marticorena, B., Chatenet, B., Rajot, J., Traoré, S., Coulibaly, M., Diallo, A., II, K., Maman, A., T, Nd., and Zakou, A.: Temporal variability of mineral dust concentrations over West Africa: Analyses of a pluriannual monitoring from the AMMA Sahelian Dust Transect, Atmospheric Chem. Phys., 10, 8899–8915, https://doi.org/10.5194/acp-10-8899-2010, 2010.

Middleton, N. J. and Goudie, A. S.: Saharan dust: sources and trajectories, Trans. Inst. Br. Geogr., 26, 165–181, https://doi.org/10.1111/1475-5661.00013, 2001.

Miller, R. L. and Tegen, I.: Climate Response to Soil Dust Aerosols, J. Clim., 11, 3247–3267, https://doi.org/10.1175/1520-0442(1998)011<3247:CRTSDA>2.0.CO;2, 1998.

Mills, M. M., Ridame, C., Davey, M., La Roche, J., and Geider, R. J.: Iron and phosphorus co-limit nitrogen fixation in the eastern tropical North Atlantic, Nature, 429, 292–294, https://doi.org/10.1038/nature02550, 2004.

Nakajima, T., Higurashi, A., Kawamoto, K., and Penner, J. E.: A possible correlation between satellite-derived cloud and aerosol microphysical parameters, Geophys. Res. Lett., 28, 1171–1174, https://doi.org/10.1029/2000GL012186, 2001.

Oke, A. M. C., Dunkerley, D., and Tapper, N. J.: Willy-willies in the Australian landscape: Sediment transport characteristics, J. Arid Environ., 71, 216–228, https://doi.org/10.1016/j.jaridenv.2007.03.014, 2007.

Okin, G. S., Mahowald, N., Chadwick, O. A., and Artaxo, P.: Impact of desert dust on the biogeochemistry of phosphorus in terrestrial ecosystems, Glob. Biogeochem. Cycles, 18, https://doi.org/10.1029/2003GB002145, 2004.

O'Neill, N. T., Eck, T. F., Smirnov, A., Holben, B. N., and Thulasiraman, S.: Spectral discrimination of coarse and fine mode optical depth, J. Geophys. Res. Atmospheres, 108, https://doi.org/10.1029/2002JD002975, 2003.

Osipov, S., Stenchikov, G., Brindley, H., and Banks, J.: Diurnal cycle of the dust instantaneous direct radiative forcing over the Arabian Peninsula, Atmospheric Chem. Phys., 15, 9537–9553, https://doi.org/10.5194/acp-15-9537-2015, 2015.

Pal, S., Lee, T. R., Phelps, S., and De Wekker, S. F. J.: Impact of atmospheric boundary layer depth variability and wind reversal on the diurnal variability of aerosol concentration at a valley site, Sci. Total Environ., 496, 424–434, https://doi.org/10.1016/j.scitotenv.2014.07.067, 2014.

Penner, J. E., Andreae, M. O., Annegarn, H., Barrie, L., Feichter, J., Hegg, D., Jayaraman, A., Leaitch, R., Murphy, D., Nganga, J., and Pitari, G.: Aerosols, their Direct and Indirect Effects, Clim. Change 2001 Sci. Basis Contrib. Work. Group Third Assess. Rep. Intergov. Panel Clim. Change, 289–348, 2001.

Pernin, J., Armante, R., Chédin, A., Crevoisier, C., and Scott, N. A.: Detection of clouds and aerosols over land and sea by day and night from hyperspectral observations in the thermal infrared, in: 3rd IASI conference, Hyères, France, 4–8, 2013.

Petäjä, T., Järvi, L., Kerminen, V.-M., Ding, A. J., Sun, J. N., Nie, W., Kujansuu, J., Virkkula, A., Yang, X., Fu, C. B., Zilitinkevich, S., and Kulmala, M.: Enhanced air pollution via aerosol-boundary layer feedback in China, Sci. Rep., 6, 18998, https://doi.org/10.1038/srep18998, 2016.

Peyridieu, S., Chédin, A., Tanré, D., Capelle, V., Pierangelo, C., Lamquin, N., and Armante, R.: Saharan dust infrared optical depth and altitude retrieved from AIRS: a focus over North Atlantic – comparison to MODIS and CALIPSO, Atmospheric Chem. Phys., 10, 1953–1967, https://doi.org/10.5194/acp-10-1953-2010, 2010.

Peyridieu, S., Chédin, A., Capelle, V., Tsamalis, C., Pierangelo, C., Armante, R., Crevoisier, C., Crépeau, L., Siméon, M., Ducos, F., and Scott, N. A.: Characterisation of dust aerosols in the infrared from IASI and comparison with PARASOL, MODIS, MISR, CALIOP, and AERONET observations, Atmospheric Chem. Phys., 13, 6065–6082, https://doi.org/10.5194/acp-13-6065-2013, 2013.

Pierangelo, C., Chédin, A., Heilliette, S., Jacquinet-Husson, N., and Armante, R.: Dust altitude and infrared optical depth from AIRS, Atmospheric Chem. Phys., 4, 1813–1822, https://doi.org/10.5194/acp-4-1813-2004, 2004.

Prospero, J. M., Ginoux, P., Torres, O., Nicholson, S. E., and Gill, T. E.: Environmental Characterization of Global Sources of Atmospheric Soil Dust Identified with the Nimbus 7 Total Ozone Mapping Spectrometer (toms) Absorbing Aerosol Product, Rev. Geophys., 40, 2-1-2–31, https://doi.org/10.1029/2000RG000095, 2002.

Pu, B. and Ginoux, P.: How reliable are CMIP5 models in simulating dust optical depth?, Atmospheric Chem. Phys., 18, 12491–12510, https://doi.org/10.5194/acp-18-12491-2018, 2018.

Pu, B., Ginoux, P., Guo, H., Hsu, N. C., Kimball, J., Marticorena, B., Malyshev, S., Naik, V., O'Neill, N. T., Pérez García-Pando, C., Paireau, J., Prospero, J. M., Shevliakova, E., and Zhao, M.: Retrieving the global distribution of the threshold of wind erosion from satellite data and implementing it into the Geophysical Fluid Dynamics Laboratory land–atmosphere model (GFDL AM4.0/LM4.0), Atmospheric Chem. Phys., 20, 55–81, https://doi.org/10.5194/acp-20-55-2020, 2020.

Randles, C. A., Da Silva, A. M., Buchard, V., Colarco, P. R., Darmenov, A., Govindaraju, R., Smirnov, A., Holben, B., Ferrare, R., Hair, J., Shinozuka, Y., and Flynn, C. J.: The MERRA-2 Aerosol Reanalysis, 1980 – onward, Part I: System Description and Data Assimilation Evaluation, J. Clim., 30, 6823–6850, https://doi.org/10.1175/JCLI-D-16-0609.1, 2017.

Redelsperger, J.-L., Thorncroft, C. D., Diedhiou, A., Lebel, T., Parker, D. J., and Polcher, J.: African Monsoon Multidisciplinary Analysis: An International Research Project and Field Campaign, Bull. Am. Meteorol. Soc., 87, 1739–1746, https://doi.org/10.1175/BAMS-87-12-1739, 2006.

Rezazadeh, M., Irannejad, P., and Shao, Y.: Climatology of the Middle East dust events, Aeolian Res., 10, 103–109, https://doi.org/10.1016/j.aeolia.2013.04.001, 2013.

Rosenfield, J. E., Considine, D. B., Meade, P. E., Bacmeister, J. T., Jackman, C. H., and Schoeberl, M. R.: Stratospheric effects of Mount Pinatubo aerosol studied with a coupled two-dimensional model, J. Geophys. Res. Atmospheres, 102, 3649–3670, https://doi.org/10.1029/96JD03820, 1997.

Schepanski, K., Tegen, I., Laurent, B., Heinold, B., and Macke, A.: A new Saharan dust source activation frequency map derived from MSG-SEVIRI IR-channels, Geophys. Res. Lett., 34, https://doi.org/10.1029/2007GL030168, 2007.

Schepanski, K., Tegen, I., Todd, M. C., Heinold, B., Bönisch, G., Laurent, B., and Macke, A.: Meteorological processes forcing Saharan dust emission inferred from MSG-SEVIRI observations of subdaily dust source activation and numerical models, J. Geophys. Res. Atmospheres, 114, https://doi.org/10.1029/2008JD010325, 2009.

Schmetz, J., Pili, P., Tjemkes, S., Just, D., Kerkmann, J., Rota, S., and Ratier, A.: AN INTRODUCTION TO METEOSAT SECOND GENERATION (MSG), Bull. Am. Meteorol. Soc., 83, 977–992, https://doi.org/10.1175/1520-0477(2002)083<0977:AITMSG>2.3.CO;2, 2002.

Schütz, L.: Long Range Transport of Desert Dust with Special Emphasis on the Sahara*, Ann. N. Y. Acad. Sci., 338, 515–532, https://doi.org/10.1111/j.1749-6632.1980.tb17144.x, 1980.

Siméoni, D., Singer, C., and Chalon, G.: Infrared atmospheric sounding interferometer, Acta Astronaut., 40, 113–118, https://doi.org/10.1016/S0094-5765(97)00098-2, 1997.

Sinclair, P. C.: General Characteristics of Dust Devils, J. Appl. Meteorol. Climatol., 8, 32–45, https://doi.org/10.1175/1520-0450(1969)008<0032:GCODD>2.0.CO;2, 1969.

Smirnov, A., Holben, B. N., Eck, T. F., Slutsker, I., Chatenet, B., and Pinker, R. T.: Diurnal variability of aerosol optical depth observed at AERONET (Aerosol Robotic Network) sites, Geophys. Res. Lett., 29, 30-1-30–4, https://doi.org/10.1029/2002GL016305, 2002.

Smirnov, A., Zhuravleva, T. B., Segal-Rosenheimer, M., and Holben, B. N.: Limitations of AERONET SDA product in presence of cirrus clouds, J. Quant. Spectrosc. Radiat. Transf., 206, 338–341, https://doi.org/10.1016/j.jqsrt.2017.12.007, 2018.

Strong, J. D. O., Vecchi, G. A., and Ginoux, P.: The Climatological Effect of Saharan Dust on Global Tropical Cyclones in a Fully Coupled GCM, J. Geophys. Res. Atmospheres, 123, 5538–5559, https://doi.org/10.1029/2017JD027808, 2018.

Su, T., Li, Z., Li, C., Li, J., Han, W., Shen, C., Tan, W., Wei, J., and Guo, J.: The significant impact of aerosol vertical structure on lower atmosphere stability and its critical role in aerosol–planetary boundary layer (PBL) interactions, Atmospheric Chem. Phys., 20, 3713–3724, https://doi.org/10.5194/acp-20-3713-2020, 2020.

Swap, R., Garstang, M., Greco, S., Talbot, R., and Kållberg, P.: Saharan dust in the Amazon Basin, Tellus B, 44, 133–149, https://doi.org/10.1034/j.1600-0889.1992.t01-1-00005.x, 1992.

Swap, R., Ulanski, S., Cobbett, M., and Garstang, M.: Temporal and spatial characteristics of Saharan dust outbreaks, J. Geophys. Res. Atmospheres, 101, 4205–4220, https://doi.org/10.1029/95JD03236, 1996.

Tanaka, T. Y. and Chiba, M.: A numerical study of the contributions of dust source regions to the global dust budget, Glob. Planet. Change, 52, 88–104, https://doi.org/10.1016/j.gloplacha.2006.02.002, 2006.

Tegen, I. and Fung, I.: Modeling of mineral dust in the atmosphere: Sources, transport, and optical thickness, J. Geophys. Res. Atmospheres, 99, 22897–22914, https://doi.org/10.1029/94JD01928, 1994.

Todd, M. C. and Cavazos-Guerra, C.: Dust aerosol emission over the Sahara during summertime from Cloud-Aerosol Lidar with Orthogonal Polarization (CALIOP) observations, Atmos. Environ., 128, 147–157, https://doi.org/10.1016/j.atmosenv.2015.12.037, 2016.

Todd, M. C., Washington, R., Raghavan, S., Lizcano, G., and Knippertz, P.: Regional Model Simulations of the Bodélé Low-Level Jet of Northern Chad during the Bodélé Dust Experiment (BoDEx 2005), J. Clim., 21, 995–1012, https://doi.org/10.1175/2007JCLI1766.1, 2008.

Tulet, P., Crahan-Kaku, K., Leriche, M., Aouizerats, B., and Crumeyrolle, S.: Mixing of dust aerosols into a mesoscale convective system: Generation, filtering and possible feedbacks on ice anvils, Atmospheric Res., 96, 302–314, https://doi.org/10.1016/j.atmosres.2009.09.011, 2010.

Vandenbussche, S., Callewaert, S., Schepanski, K., and De Mazière, M.: North African mineral dust sources: new insights from a combined analysis based on 3D dust aerosol distributions, surface winds and ancillary soil parameters, Atmospheric Chem. Phys., 20, 15127–15146, https://doi.org/10.5194/acp-20-15127-2020, 2020.

Wang, J., Xia, X., Wang, P., and Christopher, S. A.: Diurnal variability of dust aerosol optical thickness and Angström exponent over dust source regions in China, Geophys. Res. Lett., 31, https://doi.org/10.1029/2004GL019580, 2004.

Washington, R., Todd, M. C., Engelstaedter, S., Mbainayel, S., and Mitchell, F.: Dust and the low-level circulation over the Bodélé Depression, Chad: Observations from BoDEx 2005, J. Geophys. Res. Atmospheres, 111, https://doi.org/10.1029/2005JD006502, 2006.

Winker, D., Hunt, W., and Weimer, C.: The on-orbit performance of the CALIOP LIDAR on CALIPSO, 10566, 105661H, https://doi.org/10.1117/12.2308248, 2017.

Winker, D. M., Vaughan, M. A., Omar, A., Hu, Y., Powell, K. A., Liu, Z., Hunt, W. H., and Young, S. A.: Overview of the CALIPSO Mission and CALIOP Data Processing Algorithms, J. Atmospheric Ocean. Technol., 26, 2310–2323, https://doi.org/10.1175/2009JTECHA1281.1, 2009a.

Winker, D. M., Vaughan, M. A., Omar, A., Hu, Y., Powell, K. A., Liu, Z., Hunt, W. H., and Young, S. A.: Overview of the CALIPSO Mission and CALIOP Data Processing Algorithms, J. Atmospheric Ocean. Technol., 26, 2310–2323, https://doi.org/10.1175/2009JTECHA1281.1, 2009b.

Wong, S. and Dessler, A. E.: Suppression of deep convection over the tropical North Atlantic by the Saharan Air Layer, Geophys. Res. Lett., 32, https://doi.org/10.1029/2004GL022295, 2005.

Yang, Y., Russell, L. M., Lou, S., Liao, H., Guo, J., Liu, Y., Singh, B., and Ghan, S. J.: Dust-wind interactions can intensify aerosol pollution over eastern China, Nat. Commun., 8, 15333, https://doi.org/10.1038/ncomms15333, 2017.

Yu, H., Chin, M., Winker, D. M., Omar, A. H., Liu, Z., Kittaka, C., and Diehl, T.: Global view of aerosol vertical distributions from CALIPSO lidar measurements and GOCART simulations: Regional and seasonal variations, J. Geophys. Res. Atmospheres, 115, https://doi.org/10.1029/2009JD013364, 2010.

Yu, H., Chin, M., Yuan, T., Bian, H., Remer, L. A., Prospero, J. M., Omar, A., Winker, D., Yang, Y., Zhang, Y., Zhang, Z., and Zhao, C.: The fertilizing role of African dust in the Amazon rainforest: A first multiyear assessment based on data from Cloud-Aerosol Lidar and Infrared Pathfinder Satellite Observations, Geophys. Res. Lett., 42, 1984–1991, https://doi.org/10.1002/2015GL063040, 2015.

Yu, H., Tan, Q., Chin, M., Remer, L. A., Kahn, R. A., Bian, H., Kim, D., Zhang, Z., Yuan, T., Omar, A. H., Winker, D. M., Levy, R. C., Kalashnikova, O., Crepeau, L., Capelle, V., and Chédin, A.: Estimates of African Dust Deposition Along the Trans-Atlantic Transit Using the Decadelong Record of Aerosol Measurements from CALIOP, MODIS, MISR, and IASI, J. Geophys. Res. Atmospheres, 124, 7975–7996, https://doi.org/10.1029/2019JD030574, 2019.

Yu, Y., Notaro, M., Kalashnikova, O. V., and Garay, M. J.: Climatology of summer Shamal wind in the Middle East, J. Geophys. Res. Atmospheres, 121, 289–305, https://doi.org/10.1002/2015JD024063, 2016.

Yu, Y., Kalashnikova, O. V., Garay, M. J., Lee, H., Choi, M., Okin, G. S., Yorks, J. E., Campbell, J. R., and Marquis, J.: A global analysis of diurnal variability in dust and dust mixture using CATS observations, Atmospheric Chem. Phys., 21, 1427–1447, https://doi.org/10.5194/acp-21-1427-2021, 2021.

Zheng, J., Zhang, Z., Garnier, A., Yu, H., Song, Q., Wang, C., Dubuisson, P., and Di Biagio, C.: The thermal infrared optical depth of mineral dust retrieved from integrated CALIOP and IIR observations, Remote Sens. Environ., 270, 112841, https://doi.org/10.1016/j.rse.2021.112841, 2022.

Zhou, L., Tian, Y., Wei, N., Ho, S., and Li, J.: Rising Planetary Boundary Layer Height over the Sahara Desert and Arabian Peninsula in a Warming Climate, J. Clim., 34, 4043–4068, https://doi.org/10.1175/JCLI-D-20-0645.1, 2021.